Fluorophosphates: Next Generation Cathode Materials for Rechargeable Batteries

ADVANCED ENERGY MATERIALS
www.advenergymat.de

Fluorophosphates: Next Generation Cathode Materials for Rechargeable Batteries

Lalit Sharma, Shashishekar P. Adiga, Husam N. Alshareef, and Prabeer Barpanda*

Cost, safety, and cycle life have emerged as prime concerns to build robust batteries to cater to the global energy demand. These concerns are impacted by all battery components, but the realizable energy density of lithium-ion batteries (LIBs)is limited by the performance of cathodes. Thus, cathode materials have a significant role to play in advancing the performance and economics of secondary batteries. To realize next generation Li-ion and post Li-ion batteries, a variety of cathode insertion materials have been explored, but finding a cost effective and stable cathode material that can deliver high energy density has been a daunting task. Oxide cathode materials are ubiquitous in commercial applications, as they can deliver high capacity. In comparison, polyanionic insertion materials can offer tuneable (high) redox potential, operational safety, and structural as well as thermal stability. Indeed, a wide range of polyanionic materials like phosphates, borates, sulfates, and their complexes have been reported. In this article, alkali metal fluorophosphates class of polyanionic cathodes for secondary batteries is discussed. The various reported fluorophosphate insertion materials are discussed in terms of their electrochemical and electrocatalytic properties. The historical overview, recent progress, and remaining challenges for polyanionic fluorophosphates are presented along with suggested future research directions and potential application.

1. Introduction

Energy has emerged as one of the prime challenges of the 21st century. The overdependence on fossil fuels and carbonaceous materials for energy needs have resulted in an increase in carbon dioxide emissions to alarming levels in the earth's atmosphere. At the same time, the fossil fuel reserves are steadily depleting. These realities have triggered significant efforts to harness renewable energy sources like hydro, solar, geothermal, or tidal energy that are intermittent in nature. Economic and sustainable energy storage devices can be coupled with renewable energy generators to realize uninterrupted energy supply. In this sector, rechargeable batteries form the most viable energy storage devices. Today, lithium-ion batteries dominate the electronics market due to their high volumetric and specific energy density.[1–5] The manifold consumption of lithium resources due to the booming multibillion-dollar industry and limited global lithium reserves have raised concerns over the future supply of Li-based precursors to cater to the large scale production of lithium-ion batteries. To alleviate this issue, various alternatives using earth-abundant elements (e.g., monovalent Na^+/K^+ and multivalent $Mg^{2+}/Ca^{2+}/Al^{3+}$) have been proposed to replace LIBs.[6–10]

The energy density of batteries is limited by the performance of cathodes. Thus, over the last five decades, three major types of insertion materials have been examined as cathodes for secondary batteries: layered transition metal oxides, Mn-based spinels, and polyanion type materials (**Figure 1**a). 2D layered transition metal oxides have been extensively studied, but issues like oxygen loss at high potentials raise safety concerns and hence oxides like $LiCoO_2$ or $LiNi_{1-x-y}Co_xMn_yO_2$ ($x < 1$, $y < 1$) are mainly limited to small portable electronics. Though oxides deliver high energy density, they have lower redox potentials due to highly covalent M—O bonding character.[11] This issue can be evaded by implementing 3D polyanionic cathode materials with tuneable (high) redox potential along with structural/thermal stability leading to safe battery operation.[12,13] Plethora of insertion materials have been reported with different polyanionic subunits $[(XO_4)_m^{n-}$: X = B, P, Si, S, W, Mo, As, Ti, V].[14–16] The high (Pauling's) electronegativity of the X atom increases the ionic character of redox metal species enhancing their redox potentials. Variety of insertion materials have been reported by combining different polyanionic subunits (e.g., PO_4CO_3) or by combining polyanionic units with other electronegative elements (e.g., SO_4F) (Figure 1). One such attractive class of cathodes is alkali metal fluorophosphates with high redox potentials stemming from the electronegativity of fluorine. Utilizing this concept, Barker et al. first reported $LiVPO_4F$ as a 4.1 V cathode for Li-ion batteries (around 2003),

L. Sharma, Prof. P. Barpanda
Faraday Materials Laboratory
Materials Research Center
Indian Institute of Science
C. V. Raman Avenue, Bangalore 560012, India
E-mail: prabeer@iisc.ac.in
Dr. S. P. Adiga
Materials and Simulations Group (SAIT-INDIA)
Samsung R&D Institute
Bangalore 560037, India
Prof. H. N. Alshareef
Materials Science and Engineering
King Abdullah University of Science and Technology
Thuwal 23955-6900, Saudi Arabia
The ORCID identification number(s) for the author(s) of this article can be found under https://doi.org/10.1002/aenm.202001449.

DOI: 10.1002/aenm.202001449

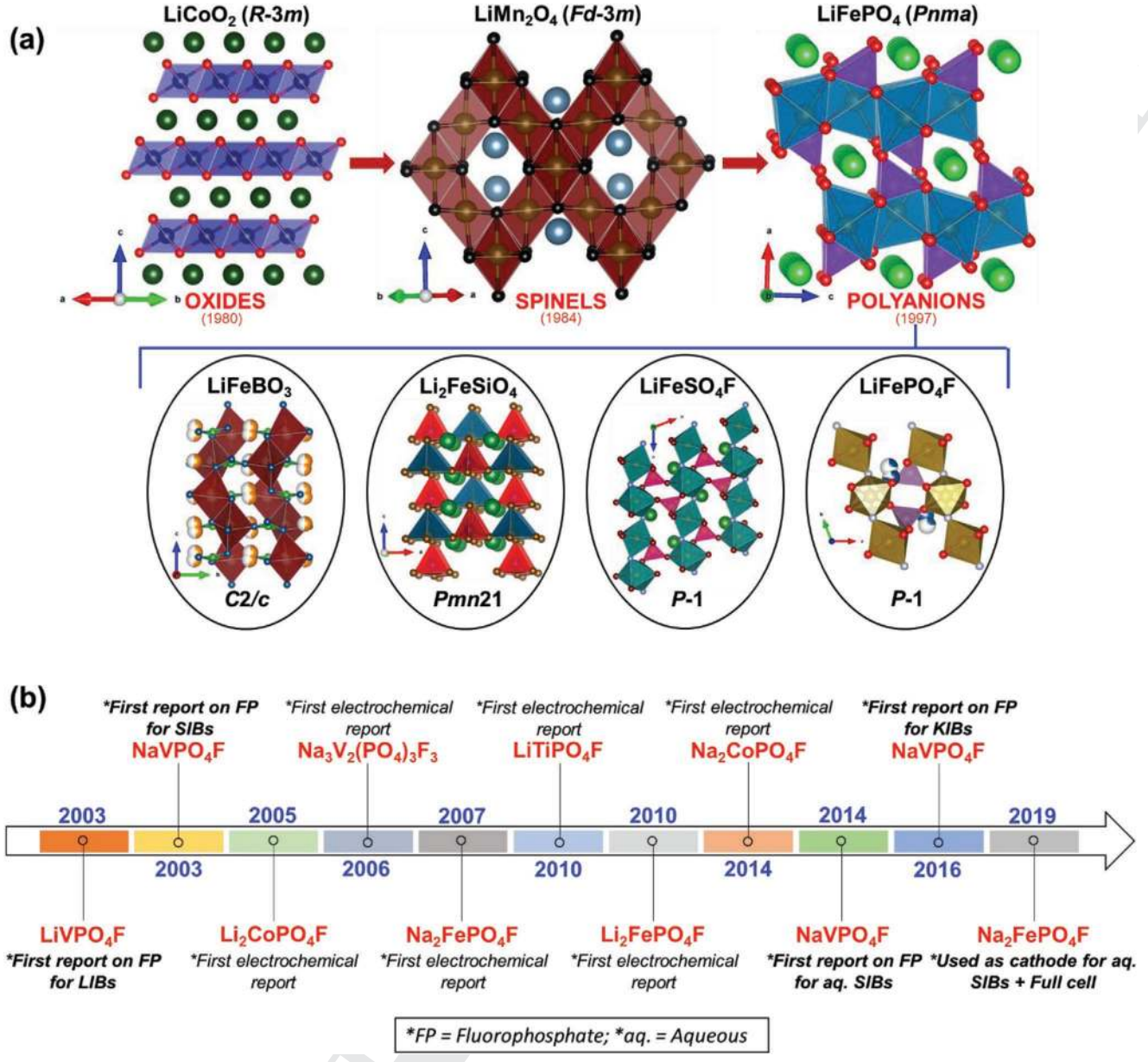

Figure 1. a) Historical development of cathode materials for secondary batteries from oxides to polyanions. (Top) Three major classes of cathode materials developed in the past forty years: oxides, spinels, and polyanions. (Bottom) Polyanionic materials adopt diverse crystal structure based on the type of polyanionic chemistry and constituent transition metals. b) Timeline depicting some key developments in the field of fluorophosphate cathode materials for Li-, Na-, and K-ion batteries.

which opened the floodgate of reports on various fluorophosphate cathodes.[17–22] Apart from earth-abundant Fe-based multifunctional end-member, several fluorophosphates have been shown to involve multiple electron reaction. Thus, it has been possible to realize fluorophosphates as both cathode and anode candidates, which can be exploited as both cathode and anode to form symmetric batteries. Off late, fluorophosphate family have been extended to Na-ion and K-ion batteries with high voltage operation. Figure 1b depicts some key milestones in the saga of fluorophosphate cathodes for lithium, sodium and potassium ion batteries. The structure and electrochemical activity of various alkali metal fluorophosphates have been summarized in **Table 1**.

Parallel to nonaqueous (organic electrolytes based) batteries, environmentally benign and economic batteries can be fabricated using aqueous electrolytes offering superior ionic conductivity, roundtrip efficiency and rate kinetics.[23] Dahn et al. first reported the concept of aqueous LIBs and since then many battery insertion materials have been implemented in aqueous media.[24–28] Additionally, exploiting the transition metal redox centers, these fluorophosphate intercalation materials can be employed as low cost electrocatalysts suitable for metal–air batteries. This review provides detailed outlook at the recent advances in exploration of fluorophosphate class of polyanionic insertion materials, which are so versatile that they can be

Table 1. Overview of fluorophosphate based cathode materials for lithium, sodium, and potassium on batteries (C, carbon; rGO, reduced graphene oxide; CTR, carbo thermal reduction; CNT, carbon nanotube; MWCNT, multiwalled carbon nanotube; SWCNT, single-walled carbon nano tube).

Material	Synthesis route	Structure	Electrolyte used	Capacity reported (theoretical capacity) mAh g^{-1}	Reference
$LiVPO_4F$	Carbothermal reduction	Triclinic	1 M $LiPF_6$ EC–DMC	115 (156)	[17]
$LiVPO_4F$	Solid-state	Triclinic	1 M $LiPF_6$ EC–DMC	155 (156)	[59]
$LiVPO_4F$	Carbothermal reduction	Triclinic	1 M $LiPF_6$ EC–DMC	140 (156)	[61]
$LiVPO_4F$	Solution method	Triclinic	1 M $LiPF_6$ EC–DMC	152.7 (156)	[68]
$LiVPO_4F$/N–C	Sol–gel	Triclinic	1 M $LiPF_6$ EC–DMC	142.1 (156)	[69]
G-$LiVPO_4F$/C	Sol–gel	Triclinic	1 M $LiPF_6$ EC–DMC	151.6 (156)	[70]
Li_3PO_4 coated $LiVPO_4F$	Solution method	Triclinic	1 M $LiPF_6$ EC–EMC–DMC	134 (156)	[73]
Polyaniline coated $LiVPO_4F$	Sol–gel	Triclinic	1 M $LiPF_6$ EC–DMC	149.3 (156)	[76]
Cr doped $LiVPO_4F$	Modified CTR	Triclinic	1 M $LiPF_6$ EC–DMC	143.5 (156)	[78]
$LiV_{0.96}Mn_{0.04}PO_4F$	Carbothermal reduction	Triclinic	1 M $LiPF_6$ EC–DMC	139 (156)	[79]
Ti doped $LiVPO_4F$	Modified CTR	Triclinic	1 M $LiPF_6$ EC–DMC	128 (156)	[82]
$LiVPO_4F$@C	Sol–gel + solid state	Triclinic	1 M $LiPF_6$ EC–DMC	147.9 (156)	[84]
$Li_5V(PO_4)_2F_2$/C	Dimensional reduction	Monoclinic	1 M $LiPF_6$ EC–DMC	88 (170)	[90]
$Li_5V(PO_4)_2F_2$/C nanocomposite	Optimized solid state	Monoclinic	1 M $LiPF_6$ EC–DMC	70 (85)	[92]
$LiFePO_4F$	Ionothermal	Triclinic	1 M $LiPF_6$ EC–DMC	128.38 (152)	[95]
$LiFePO_4F$	Solid-state	Triclinic	1 M $LiPF_6$ EC–DMC	145 (152)	[96]
$LiFePO_4F$/C	Solid-state	Triclinic	1 M $LiPF_6$ EC–DEC	131 (152)	[97]
$LiFePO_4F$	Solid-state	Triclinic	1 M $LiPF_6$ EC–DEC	119 (152)	[98]
$LiFePO_4F$	Phosphorous acid route	Triclinic	1 M $LiPF_6$ EC–DMC	146 (152)	[99]
$LiFePO_4F$	Fluorolytic sol–gel	Triclinic	1 M $LiPF_6$ EC–PC–DMC	125 (152)	[100]
$LiTiPO_4F$	Ionothermal	Triclinic	1 M $LiPF_6$ EC–DMC	150 (159)	[95]
$LiTiPO_4F$/C	Ionothermal	Triclinic	1 M $LiPF_6$ EC–PC–DMC	157 (159)	[103]
Li_2CoPO_4F	Solid-state	Ortho-rhombic	1 M $LiPF_6$ EMS-DMS	109 (143.47)	[113]
Li_2CoPO_4F/C	Sol–gel	Ortho-rhombic	1 M $LiPF_6$ EC–DMC or EMS/DMS	132 (143.47)	[114]
Li_2CoPO_4F/C	Solvothermal	Ortho-rhombic	1 M $LiPF_6$ DMC–FEC	143 (143.47)	[115]
Li_2CoPO_4F/C	Two-step reaction	Ortho-rhombic	1 M $LiPF_6$ DMC–FEC	120 (143.47)	[116]
ZrO_2 coated Li_2CoPO_4F	Conventional solution method	Ortho-rhombic	1 M $LiPF_6$ EC–DMC	127 (143.47)	[118]
Nano SiO_2@Li_2CoPO_4F	Hydrothermal method	Ortho-rhombic	1 M $LiPF_6$ EC–DMC	112.4 (143.47)	[119]
$Li_2Ni_{0.98}Co_{0.02}PO_4F$	–	Ortho-rhombic	1 M $LiBF_4$ EC–DMC–sebaconitrile	≈6 µAh (143.6)	[126]
$NaVPO_4F$/C	Solid-state	Monoclinic	1 M $NaClO_4$ EC–DMC	97.8 (142.6)	[20]
$NaVPO_4F$	Solid-state	Tetragonal	1 M $NaClO_4$ EC–DMC	78 (142.6)	[52]
$NaVPO_4F$	Soft-template method	Monoclinic	1 M $NaClO_4$ EC–PC	133 (142.6)	[132]
$NaVPO_4F$/C	Hydrothermal method	Tetragonal	1 M $NaClO_4$ EC–DEC	121 (142.6)	[133]
$NaVPO_4F$/C	Electro-spinning	Monoclinic	1 M $NaClO_4$ PC–FEC	126.3 (142.6)	[134]
$NaVPO_4F$/C	Sol–gel		1 M $NaClO_4$ EC–DEC–FEC	106 (142.6)	[135]
$NaVPO_4F$/C	Molten state blending	Monoclinic	1 M $NaClO_4$ EC–DEC–FEC	135 (142.6)	[136]
$NaVPO_4F$/C	Solution method	Monoclinic	1 M $NaClO_4$ PC–FEC	111 (142.6)	[137]
$Na_3V_2(PO_4)_2F_3$	Solid-state	Tetragonal	1 M $LiPF_6$ EC–DMC	120 (128.2)	[22]
$Na_3V_2(PO_4)_2F_3$	Solid-state	Tetragonal	1 M $NaClO_4$ PC	108 (128.2)	[146]
$Na_3V_2(PO_4)_2F_3$	Carbothermal reduction	Tetragonal	1 M $NaClO_4$ PC	111.6 (128.2)	[147]

Table 1. Continued.

Material	Synthesis route	Structure	Electrolyte used	Capacity reported (theoretical capacity) mAh g^{-1}	Reference
$Na_3V_2(PO_4)_2F_3$	Solid-state	Tetragonal	1 M $NaPF_6$ EC–PC–DMC	200 (192.44)	[152]
$Na_3V_2(PO_4)_2F_3$@C	Sol–gel	Tetragonal	1 M $NaClO_4$ EC–PC–FEC	130 (128.2)	[153]
$Na_3V_2(PO_4)_2F_3$@C/CNT	Spray drying	Tetragonal	1 M $NaClO_4$ EC–PC–FEC	113 (128.2)	[154]
$Na_3V_2(PO_4)_2F_3$/C@RGO	Sol–gel	Tetragonal	1 M $NaClO_4$ EC–DMC	124.5 (128.2)	[155]
$Na_3V_2(PO_4)_2F_3$@C	Solution Combustion	Tetragonal	1 M $NaClO_4$ EC–PC–FEC	120 (128.2)	[156]
K-doped $Na_3V_2(PO_4)_2F_3$@CNT	Sol–gel	Tetragonal	1 M $NaClO_4$ EC–PC–FEC	120 (128.2)	[157]
$Na_{1.5}VOPO_4F_{0.5}$	Solid-state	Tetragonal	1 M $NaClO_4$ PC	87 (156)	[161]
$Na_3(VO)_2(PO_4)_2F$	Hydrothermal	Tetragonal	1 M $NaClO_4$ EC–PC	100 (156)	[164]
$Na_3(VO)_2(PO_4)_2F$-graphene	Solvothermal	Tetragonal	1 M $NaPF_6$ EC–DEC	120 (122.4)	[172]
$Na_3(VO)_2(PO_4)_2F$-MWCNT	Hydrothermal	Tetragonal	1 M $NaClO_4$ PC–FEC	98 (122.4)	[175]]
$Na_3(VO)_2(PO_4)_2F$	Solvothermal	Tetragonal	1 M $NaClO_4$ EC–DEC	120 (122.4)	[178]
RuO_2 coated $Na_3(VO)_2(PO_4)_2F$	Micro emulsion hydrothermal	Tetragonal	1 M $NaClO_4$ PC	126 (122.4)	[180]
Na_2FePO_4F	Ionothermal	Ortho-rhombic	1 M $NaClO_4$ PC	110 (124.2)	[19]
Na_2FePO_4F	Solid-state	Ortho-rhombic	1 M $NaClO_4$ PC–FEC	110 (124.2)	[184]
Na_2FePO_4F	Mechano chemical	Ortho-rhombic	1 M $LiPF_6$ EC–DMC	116 (124.2)	[185]
Na_2FePO_4F	Solution combustion	Ortho-rhombic	0.5 M $NaPF_6$ PC	100 (124.2)	[188]
Na_2FePO_4F	Soft-template + ball milling	Ortho-rhombic	1 M $NaClO_4$ EC–PC	116 (124.2)	[189]
Na_2FePO_4F/C	solvothermal	Ortho-rhombic	1 M $NaPF_6$ EC–DEC–FEC	120.1 (124.2)	[190]
Na_2FePO_4F/C	Ultrasonic spray pyrolysis	Ortho-rhombic	1 M $NaClO_4$ EC–DMC	89 (124.2)	[191]
Carbon coated Na_2FePO_4F	Green mechano chemical	Ortho-rhombic	1 M $NaClO_4$ PC–FEC	117 (124.2)	[192]
Na_2FePO_4F/rGO	Polyol	Ortho-rhombic	1 M $NaClO_4$ PC–FEC	110 (124.2)	[193]
Carbon coated Na_2FePO_4F	Solvothermal	Ortho-rhombic	1 M $NaPF_6$ EC–DEC–FEC	114.3 (124.2)	[194]
Na_2FePO_4F/CNT	Layer by layer nano assembly	Ortho-rhombic	1 M $NaClO_4$ EC–DMC	103.5 (124.2)	[195]
Na_2CoPO_4F	Solid-state	Ortho-rhombic	1 M $NaPF_6$ EC–DEC–FEC	100 (122.4)	[206]
Na_2CoPO_4F/C	Spray-drying	Ortho-rhombic	1 M $NaPF_6$ EC–DMC–FEC	107 (122.4)	[207]
Na_2MnPO_4F	Sol–gel	Monoclinic	1 M $LiPF_6$ EC–DMC	98 (124.7)	[203]
Na_2MnPO_4F/C	Spray-drying	Monoclinic	1 M $NaClO_4$ EC–PC	140 (124.7)	[208]
Na_2MnPO_4F/C	Spray-drying	Monoclinic	1 M $NaClO_4$ EC–PC	178 (124.7) @55 °C	[208]
$NaVPO_4F$	Sol–gel	Tetragonal	5 M $NaNO_3$	54 (142.6)	[209]
$Na_3(VO)_2(PO_4)_2F$-MWCNT	Hydrothermal	Tetragonal	10 M $NaClO_4$	35 (122.4)	[175]
Na_2FePO_4F	Solution combustion	Ortho-rhombic	17 M $NaClO_4$	84 (124.2)	[210]
$Na_3V_2(PO_4)_2F_3$-SWCNT	Solid-state	Tetragonal	17 M $NaClO_4$	81.3 (128.2)	[212]
$K_3V_2(PO_4)_2F_3$	Electrochemical ion exchange	Ortho-rhombic	1 M KPF_6 EC–PC	100 (115)	[213]
$KVPO_4F$	Solid state	Ortho-rhombic	0.7 M KPF_6 EC–DEC	105 (131.3)	[214]

used in (non)aqueous batteries as well as bifunctional electrocatalysts. The synthetic, structural, transport, electrochemical, electrocatalytic, and mechanistic properties are summarized for various alkali metal fluorophosphates.

2. A Brief History of Cathode Materials

The concept of battery dates back to 1748 when Benjamin Franklin coined the termed "battery." Alessandro Volta made the first electrochemical cell in 1800. Since then, this field has witnessed a drastic development in terms of chemistry and technologies. Ni–Cd and Ni–MH batteries were dominating in the early 19th century before lead-acid batteries were revived significantly in the mid-1970s. While some chemistry (e.g., Pb and Cd) were not benign in nature, all these batteries suffered from poor gravimetric/volumetric energy density. Catering the ever-growing energy demand of the 21st century world called for superior electrochemical storage technology with high energy density. The vision was realized in 1991 with the historic commercialization of lithium-ion batteries by SONY, which remains a key milestone in modern technological revolution. It triggered an exponential rise in research and development of various Li-ion and post Li-ion battery chemistry.

Ever since secondary batteries based on lithium and sodium chemistry have come into existence, research on finding superior cathode materials has been growing, especially in LIBs using graphite as anode. In such batteries, the specific capacity and energy density of the cell is limited by the cathode performance. The era of LIBs started with oxide cathodes, i.e., $LiCoO_2$ which was first reported by Goodeneough in 1980.[29] For almost 20 years, this material was used as cathode in commercialized LIBs. The properties of the oxide were later improved by doping of metal ions leading to the inception and successful commercialization of $LiNi_{0.80}Co_{0.15}Al_{0.05}O_2$ (NCA) and $LiNi_{1/3}Mn_{1/3}Co_{1/3}O_2$ (NMC) cathodes.[30,31] Spinels like $LiMn_2O_4$ were also found to have high reversible capacities at high operating potential.[32,33] However, the oxide-based materials suffer from thermal runaway at high potentials hence raising some safety issues.

Since the discovery of $LiFePO_4$ in 1997,[14] design of polyanionic materials based on transition metal-ion having 3D crystal structures have been a subject of intense research. Polyanion-based materials exhibit many advantages over oxide-based materials like robust crystal structure, high redox potential, and structural versatility (**Figure 2**). Since then, variety of materials based on different polyanionic groups have been discovered. Delmas reported the electrochemical activity in NASICON based $LiTi_2(PO_4)_3$ and $NaTi_2(PO_4)_3$ in 1987–1988.[34–36] Insertion of Li in $Fe_2(SO_4)_3$ was reported by Manthiram in 1989.[12] Armand, in 1999, demonstrated improved electrochemical performance in $LiFePO_4$ by carbon coating.[37,38] Since then, variety of synthesis techniques have been developed to optimize the morphology, grain size and resultant properties of cathode materials.[39–44] In 2001, lithium metal borates, $LiMBO_3$ (M = Fe, Mn, Co) were unveiled as potential alternative to $LiFePO_4$ due to their low molecular mass.[45] Li (de)intercalation properties of Li_2FeSiO_4 silicate was first reported by Armand and co-workers.[46,47] Pursuing (PO_4)-chemistry, pyrophosphate-based materials was also explored for their intercalation properties.[48–51] Barker proposed Na-intercalation in $NaVPO_4F$ in 2003.[52] Following this report, many vanadium-based fluorophosphates were reported for secondary batteries.[53–57] It also led to the development of layered-Na_2FePO_4F, which was first reported in 2007 by Nazar's group.[18] Notably, the crystal structures of the materials are different depending on the nature of the polyanionic groups involved. Even after extensive research over three decades, the field still stays vast open for the discovery and development of new polyanionic insertion materials.

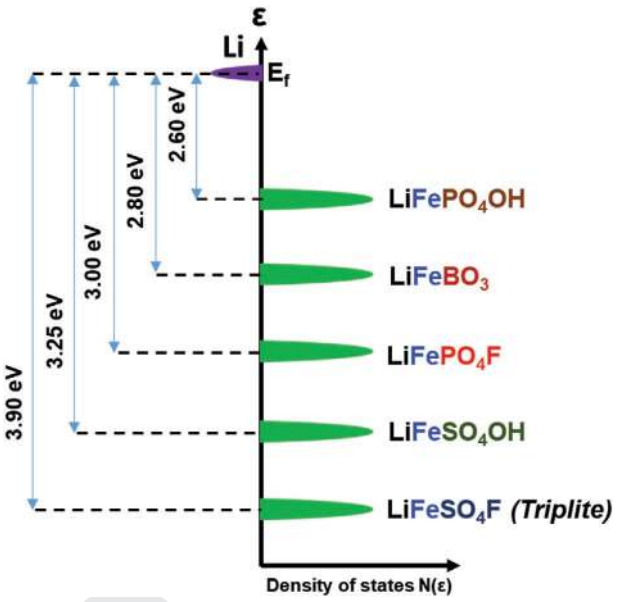

Figure 2. Change in the Mn^{+1}/Mn redox potential for different polyanionic systems as a function of electronegativity of the central atom of polyanionic groups. More electronegative polyanions deliver higher redox potential.

This review will focus on a particular class of polyanionic materials as cathodes for secondary batteries: fluorophosphates ($AMPO_4F$). This subclass of polyanionic compounds exhibits a huge potential in becoming an effective cathode material for secondary batteries, in particular, sodium-ion batteries (SIBs). The review covers fluorophosphates with various transition metals (M = V, Fe, Co, Mn, Ti, Ni). This know-how can be further extended to hydroxyphosphates ($AMPO_4OH$) taking into account the effect of anionic electronegativity (F^- vs OH^-) on the redox potential. Performance of these fluorophosphate polyanionic insertion materials is summarized in both aqueous and organic electrolytes. The commercial perspective of these materials along with some electrocatalytic studies is also discussed.

3. Fluorophosphates

3.1. Fluorophosphates for Lithium-Ion Batteries

3.1.1. Vanadium-Based Fluorophosphates

Fluorophosphates first came into existence when Barker et al. introduced $LiVPO_4F$ (LVPF) as a cathode material in 2003.[17] It

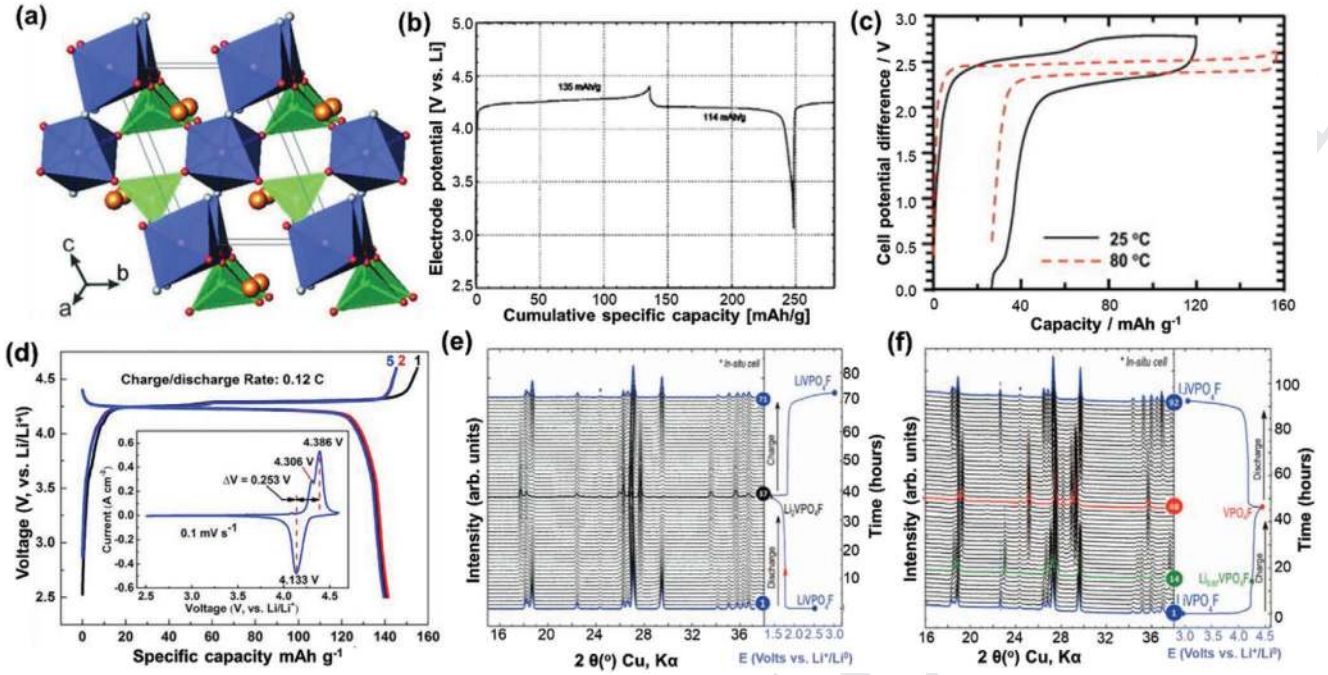

Figure 3. a) Crystal structure of tavorite $LiVPO_4F$ (LVPF) built from VO_4F_2 octahedra (blue) and PO_4 tetrahedra (green). b) The first electrochemical report of LVPF cycled in the potential range of 3–4.4 V giving a discharge capacity of 114 mAh g^{-1}. c) Cycling of LVPF symmetric cell using ionic liquid electrolyte at room temperature and 80 °C. d) Improved cyclability of LVPF on potassium doping. e, f) In situ XRD plots (2D) recorded during cycling in low-voltage and high-voltage regions respectively. a) Reproduced with permission.[77] Copyright 2015, IUCr. b) Reproduced with permission.[17] Copyright 2003, The Electrochemical Society. c) Reproduced with permission.[66] Copyright 2011, Elsevier. d) Reproduced with permission.[86] Copyright 2018, Elsevier. e,f) Reproduced with permission.[87] Copyright 2012, The Electrochemical Society.

was synthesized by a two-step carbothermal reduction method. Isostructural to $LiFePO_4OH$, it crystallizes in a triclinic structure with *P*-1 space group (s.g.) as illustrated in **Figure 3**a. The structure consists of $[VO_4F_2]$ octahedra linked together by F-atoms present at *trans* position forming chains along *c*-axis. These chains are interconnected by PO_4-groups giving rise to 3D framework. The constituent Li-ions are accommodated in two distinct sites: one being a penta-coordinated site (LiO_5) with occupancy of 18% and the second is an octahedral site (LiO_6) with 82% occupancy.[58] Later, Ateba et al. carried out careful structural analysis combining X-ray and neutron diffraction patterns and proposed single site occupancy for Li.[59] Different types of tunnels were observed in the structure resulting from the connection of different octahedra chains $[VO_4F_2]$ and PO_4 tetrahedra units with homogeneous V—F bond distances along the chains. Defects in this crystal structure were observed by Masquelier's group by means of ^7Li spin-echo nuclear magnetic resonance measurements.[60] Barker group first tested the electrochemical properties of LVPF in lithium-based cell where they obtained a capacity of 114 mAh g^{-1} when cycled between 3 and 4.4 V at C/5 rate with a discharge plateau at 4.2 V (Figure 3b).

Although they initially focused on one electron V^{4+}/V^{3+} redox activity, they later reported the presence of multivalent reactions in LVPF.[56] A capacity of 140 mAh g^{-1} was obtained with two redox plateaus at 1.8 V ($V^{3+/2+}$) and 4.2 V ($V^{4+/3+}$) having two-phase reaction. Doping of metals (e.g., Al-doping) is well-known to facilitate structural stability and hence the electrochemical performance. Barker group tried to partially substitute Al^{3+} into V^{3+} site.[61] Aluminium was chosen because i) its ionic radius is close to that of vanadium and ii) $LiAlPO_4F$ is isostructural to LVPF. Presence of Al decreased the polarization and enhanced the $V^{4+}/^{3+}$ redox potential from 4.19 to 4.28 V with improved cyclability. Al-doping helps in mitigating the issue of enhanced charge-transfer resistance at the interface of cathode and electrolyte by suppressing the formation of surface layer on cathode. It results in low polarization and increased redox potential in the electrochemical performance of Al-doped cathode materials, which has also been explained by theoretical studies.[62–65] With the material showing one electron transfer during both oxidation (4.2 V) and reduction (1.8 V) processes, a symmetric (–) $LiVPO_4F$ || $LiVPO_4F$ (+) cell was assembled.[56] This is the first example of a symmetric cell working with same anode and cathode material. In the potential window of 2.4 V, this symmetric cell delivered a reversible capacity of 130 mAh g^{-1} albeit with poor cyclability. Following, Okada group employed 1 M $LiBF_4$/$EMIBF_4$ ionic liquid electrolyte to obtain a stable and reversible symmetric cell.[66] Even at 80 °C, a discharge capacity of 120 mAh g^{-1} was obtained at a current density of 1 mA cm^{-2} as shown in Figure 3c. LVPF || graphite full cell have been demonstrated with long-range cyclability at C/2 rate, giving a capacity of more than 120 mAh g^{-1} after 200 cycles.[61] From accelerating rate calorimetry tests on delithiated LVPF sample, it is proposed that the thermal stability of the VPO_4F–$LiVPO_4F$ is comparable to $LiFePO_4$–$FePO_4$ system.[67]

The low electronic conductivity of the material limits its application in high-power density batteries. This can be improved by surface coating and cation doping. Coating materials like

graphene, Li_3PO_4, MoS_2, and polyaniline have been reported to improve the electronic and ionic conductivity.[68–76] Ion doping can change the electronic cloud structure while carbon coating can reduce the band gap and hence increase the electronic conductivity.[61,77–83] Core–shell carbon coated LVPF was prepared using sol–gel technique and a capacity of 147.9 mAh g^{-1} was obtained at 0.1 C with excellent rate capability and good cycling performance.[84] CNT decorated $LiVPO_4F$/C were synthesized using sol–gel synthesis route and a high reversible capacity of 121.1 mAh g^{-1} at 10 C rate was obtained.[85] Potassium doping into vanadium sites suppressed the formation of $Li_3V_2(PO_4)_3$ impurity and also reduced agglomerization leading to homogeneous distribution of particle size.[86] The K-doped samples showed lower polarization, reduced charge transfer resistance and improved Li^+ diffusion coefficient when compared to the pristine LVPF as shown in Figure 3d.

Ateba et al. conducted an in-depth structural investigation by employing in situ XRD analysis.[87] The low voltage region corresponding to $V^{3+/2+}$ redox exhibits a biphasic mechanism while extraction of Li in the high voltage region ($V^{4+/3+}$ redox) involves two plateaus at 4.24 and 4.28 V. The in situ XRD was recorded between 2.5 and 1.45 V during cycling and a gradual disappearance of peaks was observed with the gradual appearance of Li_2VPO_4F phase having $C2/c$ space group (Figure 3e). In the high voltage region, an inflection point corresponding to the composition of $Li_{0.67}VPO_4F$ was observed as shown in Figure 3f. This phase can be indexed to a single phase during in situ XRD study. However, from $LiVPO_4F$ to $Li_{0.67}VPO_4F$, a two-phase mechanism was noticed and similar process was observed between $Li_{0.67}VPF$ to VPO_4F endphase. Surprisingly, this was not observed during discharge with a single two-phase reaction occurring between VPO_4F and LVPF. This structural change was observed to be reversible. Evolving factor analysis (EFA) of X-ray absorption near-edge spectroscopy (XANES) showed the presence of three reversible phases during cycling: $LiVPO_4F$, Li_xVPO_4F ($x = 0.80–0.25$) and VPO_4F. No single phase $Li_{0.67}VPF$ was detected.[88] Ellis et al. isolated two end members, namely, VPO_4F and Li_2VPO_4F, obtained during cycling of LVPF. Both these end members crystallized in a monoclinic structure with $C2/c$ symmetry. There is a volumetric change of 15.9% during the two-electron transfer process. ^{6,7}Li NMR studies identified two different crystallographic sites of Li in Li_2VPO_4F, which exchange at slightly above the room temperature. Vanadyl oxyphosphate, $LiVPO_4O$ that closely relates to LVPF, has also been studied by Croguennec group. It can also exploit two redox couples $V^{5+/4+}$ at 3.95 V and $V^{4+/3+}$ at 2.3 V (vs Li/Li^+). In the high-voltage region, the material delivered an initial capacity of 78 mAh g^{-1}, which gradually increases to 135 mAh g^{-1} in 30 cycles with steady decrease in polarization.[89] In the low-voltage region, three plateaus at 2.45, 2.21, and 2.04 V (vs Li/Li^+) were observed. The structural variation during cycling was studied by in situ XRD measurements.

A new type of vanadium based fluorophosphate, $Li_5V(PO_4)_2F_2$, was introduced by Nazar group in 2006.[90] This material was synthesized by reaction of α-$Li_3V_2(PO_4)_3$ in LiF flux and consists of anisotropic 2D structure. Since it was synthesized starting from a 3D α-$Li_3V_2(PO_4)_3$, it was an interesting example of "dimensional reduction," a term first coined by Long et al. (**Figure 4**a).[91] It crystallizes in a monoclinic structure with $P2_1/c$ space group. The V–O(F) octahedra are isolated from each other but they are interconnected by corner-sharing PO_4-tetrahedra groups. The 2D sheets of VO_4F_2–PO_4 sandwich the 2D layers of lithium ions. The material has a theoretical capacity of 170 mAh g^{-1} involving two electron transfer via $V^{4+/3+}$ and $V^{5+/4+}$ redox activity. At a current rate of C/10, it delivered a capacity of 88 mAh g^{-1} when cycled between 3 and 4.5 V. A distinct $V^{4+/3+}$ redox activity was observed at 4.15 V. Upon cycling till 5.0 V, a second plateau at 4.7 V was observed stemming from $V^{5+/4+}$ redox activity. Employing ^{6}Li NMR study, six crystallographic sites for lithium were determined (Figure 4b).[92] 2D exchange spectroscopy (EXSY) study showed that Li-ions exchange along the *a*-axis but not through (100) plane. They also reported the Li-stuffed structure is not conducive for rapid Li-exchange because of high degree ordering of the Li sites and lack of vacancies. $Li_4V(PO_4)_2F_2$/carbon nanocomposite was prepared by solid-state route via chemical oxidation of $Li_5V(PO_4)_2F_2$.[93] Upon delithiation, the ionic mobility was enhanced due to creation of vacancies in the structure. ^{6,7}Li NMR coupled with 2D EXSY studies were used to characterize the structure. These vanadium-based materials, specially $LiVPO_4F$, exhibits high reversible capacity, good rate capability and excellent cycling stability. Nonetheless, they never tasted commercial success and real-life products owing to the cost and toxicity issues generally associated with vanadium-based compounds.

3.1.2. Fluorophosphates with General Formula $LiMPO_4F$ (M = Fe, Ti)

Following the discovery of $LiVPO_4F$, Barker tried to synthesize $LiMPO_4F$ (M = Fe, Co, Cr, Ti) analogs.[94] He claimed all these fluorophosphates to be isostructural and crystallizing in triclinic tavorite structure (space group *P*-1). One such analogue $LiFePO_4F$ (LFPF) stands out owing to earth-abundant Fe composition. However, its synthesis, detailed structure and potential electrochemical activity was not reported. In 2010, Tarascon group first synthesized this material employing both (dry) solid-state and (wet) ionothermal synthesis routes.[95] LFPF is isostructural to $LiVPO_4F$ and $LiFePO_4OH$, and crystallize in a triclinic framework built from FeO_4F_2 octahedra interlinked by F-atoms to form parallel chains. These parallel chains are cross-linked by PO_4-tetrahedra giving rise to a 3D framework. They observed a staircase like profile during discharge while it was missing during charge. In the same year, Nazar group also came up with solid-state synthesis of LFPF but using different precursors.[96] However, with uniform carbon coating they were able to (de)intercalate 0.96 Li^+ from the material at 3.0 V. No staircase like profile was observed in their case, rather a sloppy behavior was observed till 0.4 Li^+ intercalation followed by appearance of a two phase plateau (**Figure 5**a). Facile phase transition was confirmed by XRD study. Moreover, it showed excellent performance at a high temperature of 55 °C. Chen et al. reported an initial discharge capacity of 128 mAh g^{-1} at 1 C current rate retaining 71% of initial capacity at the end of 100 cycles (Figure 5b).[97] From impedance spectral analysis, Prabu et al. reported ionic conductivity of 0.6×10^{-7} S cm^{-1} at 27 °C that increased to 5.4×10^{-7} S cm^{-1} at 50 °C. [98] Asl reported a phosphorous acid based route for synthesis of LFPF.[99] Recently microwave-assisted fluorolytic sol–gel route

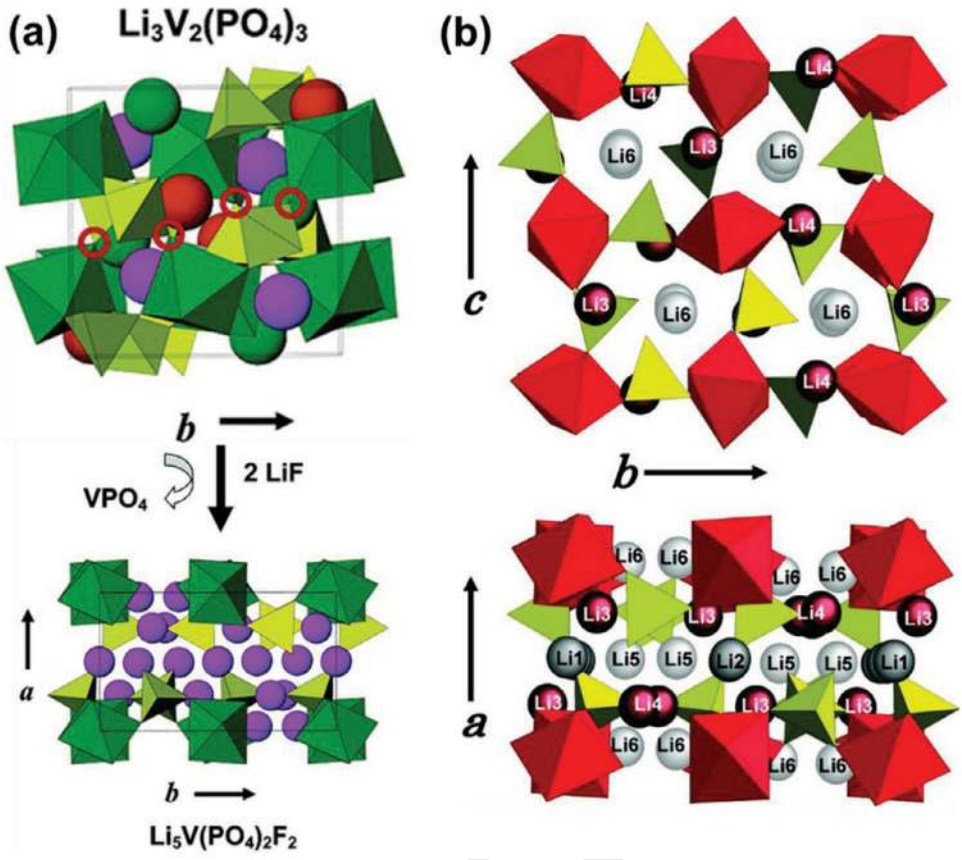

Figure 4. a) Illustration of dimensional reduction process from 3D α-$Li_3V_2(PO_4)_3$ to 2D $Li_5V(PO_4)_2F_2$ structure. b) Crystal structure showing six sites of lithium in the (100) plane and along *a*-axis. a) Reproduced with permission.[90] Copyright 2006, American Chemical Society. b) Reproduced with permission.[92] Copyright 2008, American Chemical Society.

was also reported to yield submicrometric LFPF particles.[100] Solid-solution series between $LiFePO_4F$–$LiVPO_4O$ homeotypic structures $LiFe_{1-x}V_xPO_4F_{1-\delta}O_\delta$ ($0 \le x \le 1$; $0 \le \delta \le 0.36$) and $LiFePO_4F$–$LiVPO_4F$ solid solutions $LiFe_{1-x}V_xPO_4F$ (x = 0, 0.1, 0.3, 0.5, 0.7, 0.9, 1) have been attempted.[101,102]

Tavorite mineral type $LiTiPO_4F$ (LTPF) was first reported by Tarascon group in 2010 by adopting both high-temperature solid-state synthesis (at 700 °C) as well as low-temperature ionothermal synthesis (at 260 °C) .[95] Isostructural to LFPF, it stabilizes into a triclinic structure with *P*-1 space group having slightly distorted TiO_4F_2 octahedra. These octahedra are linked together by F-atoms present at *trans*-position to form 1D chains. Adopting ionothermal synthesis route led to finer particle morphology when compared to solid-state (ceramic) synthesis,

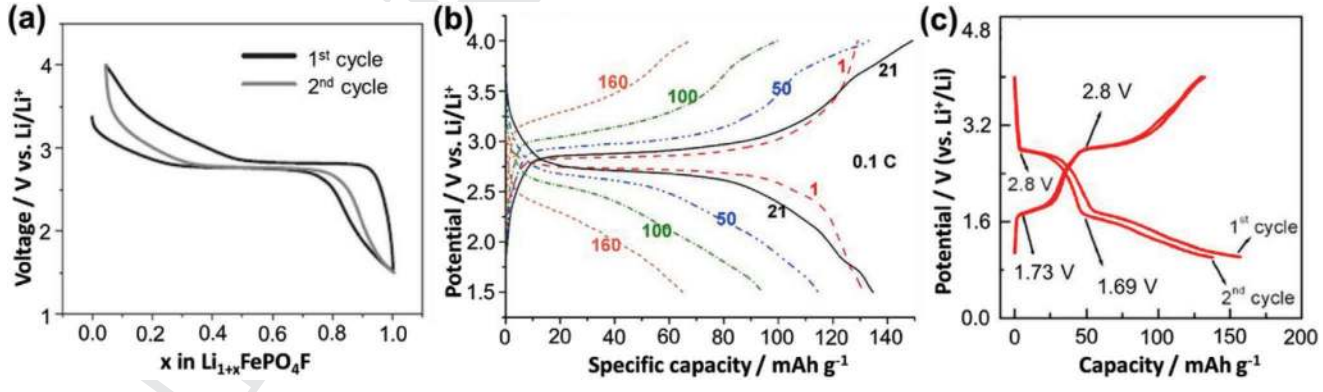

Figure 5. a) Electrochemical (dis)charge profile of tavorite $LiFePO_4F$ at C/10 current rate at room temperature. b) Electrochemical (dis)charge profile of $LiFePO_4F$ at various current rates. c) Electrochemical (dis)charge profile of $LiTiPO_4F$/C when cycled between 1.0 and 4.0 V (vs Li/Li^+) at C/15 rate. a) Reproduced with permission.[96] Copyright 2010, The Electrochemical Society. b) Reproduced with permission.[97] Copyright 2014, Elsevier. c) Reproduced with permission.[103] Copyright 2016, Wiley-VCH.

thereby delivering a reversible capacity of 150 mAh g^{-1}. The electrochemistry of the material revealed a staircase like voltage profile with reversible plateaus centered at 2.9 and 1.7 V (vs Li^+/Li) owing to multiple redox processes involving Ti during cycling. Rangaswamy et al. revisited the ionothermal synthesis to form carbon-coated LTPF compound by employing C2-OH DCA ionic liquid.[103] From cyclic voltammetry, they confirmed the presence of Ti^{3+}/Ti^{2+} and Ti^{4+}/Ti^{3+} redox couples in the voltage range of 1–4 V (vs Li^+/Li). A first discharge capacity of 157 mAh g^{-1} was obtained at C/15 rate with excellent cyclability till 200 cycles (Figure 5c). They also fabricated a full-cell with graphite as an anode delivering the first discharge capacity of 149 mAh g^{-1} and retaining 87% of the initial value at the end of 200th cycle. Effect of temperature on the half-cell properties was also studied and good cyclic behavior was observed at both low temperature (10 °C) and high temperature (55 °C) . Material stability during cycling was also confirmed by ex situ XRD. They further studied LTPF in aqueous electrolyte and reported it as an anode for aqueous LIBs in 2 M Li_2SO_4 aqueous electrolyte.[104] A new synthesis route namely reaction under autogenic pressure at elevated temperature (RAPET) was adopted. Li-rich $Li[Li_{0.2}Co_{0.3}Mn_{0.5}]O_2$ was used as a cathode for full-cell electrochemical studies. With the help of CV, the potential window was carefully optimized to +1.2 to −1.0 V. A reversible discharge capacity of 82 mAh g^{-1} was obtained at C/5 current rate corresponding to 0.52 Li^+ intercalating within anode and cathode. Singh et al. came up with another synthesis route for LTPF using direct chemical solution deposition process without any post heat treatment. It led to the development of flower like morphology.[105] A stable discharge capacity of 150 mAh g^{-1} at a rate of C/10 for the initial 10 cycles was obtained. Generally, tavorites form open frameworks capable of efficient Li^+ (de)intercalation. Thereby, tavorite structured LFPF and LTPF were found to be electrochemically active electrode materials involving stair-case type voltage profiles with excellent reversibility. Based on earth-abundant Fe and Ti chemistry, they can form economic electrodes for batteries. Nonetheless, operation at intermediate voltage (<3 V for LFPF and ≈1.1 V for LTPF vs Li^+/Li) restricts their energy density and therefore hindering in possible practical application.

3.1.3. Fluorophosphates with General Formula Li_2MPO_4F (M = Fe, Co, Mn, Ni)

These materials have attracted wide interest due to the possibility of (de)intercalating more than one lithium-ion per transition metal resulting in high energy density. Depending on the type of transition metal and synthesis approach, these materials can adopt diverse crystal structure. Phase-pure Li_2FePO_4F (L2FPF) was first obtained by Nazar group (in 2010) by chemical reduction of tavorite $LiFePO_4F$.[96] It was found to adopt an isostructural triclinic *P*-1 type structure with 8% increase in the unit cell volume. The reduction of Fe^{3+} to Fe^{2+} was confirmed by Mössbauer spectroscopy. The structure was solved by combining both X-ray and neutron diffraction patterns.[106] Overall, the corner-shared framework of $FePO_4F$ remained intact upon chemical reduction. Three crystallographically unique sites were identified for constituent Li species (**Figure 6**a). The Li1 is positioned close to the centroid of the split Li position in $LiFePO_4F$. However, due to larger size of Fe^{2+}, the site of Li1 is smaller than that in $LiFePO_4F$. The other two sites Li2 and Li3 are equally occupied by 0.5 lithium. Li2 is situated between chains of Fe octahedra that are coordinated by two fluorine and four oxygen ligands. The Li3 site is octahedrally coordinated by one fluorine and five oxygen ligands. Moreover, they observed that L2FPF obtained from reduction of $LiFePO_4F$ differs from the one obtained by ion exchange of orthorhombic Na_2FePO_4F.[18] L2FPF obtained by ion exchange in Na_2FePO_4F resulted in a layered 2D orthorhombic structure. It delivered a discharge capacity of 110 mAh g^{-1} at 3.3 V. Antipov group synthesized mixed $NaLiFePO_4F$ followed by electrochemical replacement of Na by Li to obtain Li_2FePO_4F end-product.[107] The electrochemistry showed similar behavior to that of layered Li_2FePO_4F having a solid-state regime at 3.4 V (vs Li^+/Li). The presence of antisite disorder was also studied.[108] The oxygen atoms linked to Li and P atoms result in bond misbalance when Li is extracted out of the system during charging. This misbalance is restored by Fe migration toward Li sites leading to Li/Fe antisite disorder.

The cobalt analog, Li_2CoPO_4F (L2CPF) was first reported by Okada group in 2005.[109] Employing powder (X-ray and neutron) diffraction patterns, L2CPF was found to assume an orthorhombic structure with *Pnma* space group. It consists of edge sharing CoO_4F_2 octahedra resulting in the formation of rutile like chains that are interconnected by PO_4 tetrahedra groups to give rise to a 3D structure. Being categorized as >4 V cathode material, the cycling was carried out in 1 M $LiPF_6$ in ethyl methyl sulfone (EMS) electrolyte. L2CPF was reported as 5 V cathode material with no structural changes during cycling. However, an irreversible capacity loss was observed after first cycle due to decomposition of electrolyte at higher voltages. They also studied the solubility of material in electrolyte and thermal stability of the material. The crystal structure was further solved using precession electron diffraction (PED) pattern and transmission electron microscopy (TEM).[110,111] Using PED, Fourier maps were built to identify the exact location of Li-atoms. Khasanova et al. tried to identify the structural changes happening in the material during cycling.[112] They found three crystallographic sites of lithium in the structure. Two of them (L1 and L2) were present in penta-coordinated sites (LiO_5) while the third one (L3) was present in an octahedral environment (LiO_6). From BVS calculations, L3 site was found to be tightly bonded and hence less mobile. Upon cycling in the potential window of 3.0–5.1 V (vs Li^+/Li), irreversible structural changes were observed above 4.8 V during first charge with volumetric expansion of >3 .5% (Figure 6b). They proposed the structural transformation happening due to mutual rotation of CoO_4F_2 octahedra and PO_4-tetrahedra. However, this transformation was found to assist the subsequent Li-(de)intercalation in the structure, which was further confirmed using cyclic voltammetry.[113] While one anodic peak was obtained upon charging till 5.0 V, two distinct anodic peaks were observed upon charging till 5.5 V. The presence of two peaks implies extraction of Li from two energetically distinct sites. However, these peaks merged in subsequent cycles hinting at structural relaxation happening during initial cycle. A reversible capacity of 109 mAh g^{-1} was observed when cycled between 2.0 and 5.5 V versus

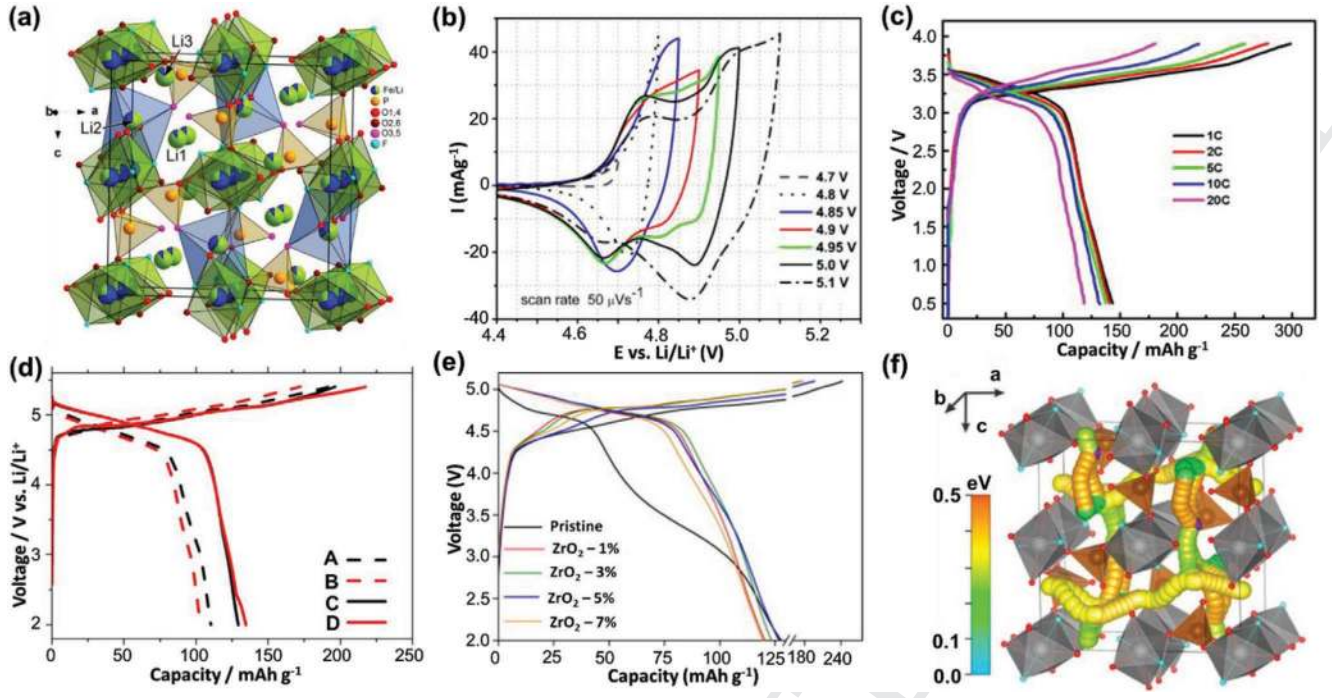

Figure 6. a) Crystal structure of Li_2FePO_4F showing three different sites of lithium. b) Cyclic voltammetry of Li_2CoPO_4F recorded in various anodic limits at a scan rate of 50 μV s^{-1} to identify the underlying structural transformations. c) Electrochemical (dis)charge profile of Li_2CoPO_4F | $Li_4Ti_5O_{12}$ full cell in $LiPF_6$ EC/DMC electrolyte at various rates. d) (Dis)charge profiles for Li_2CoPO_4F at C/5 rate when cycled between 2 and 5.4 V using A) 200 μL of 1 M $LiPF_6$ in EC/DMC, B) 200 μL of 0.5 M $LiPF_6$ in FEC/DMC, C) 50 μL of 1 M $LiPF_6$ in EC/DMC, and D) 50 μL of 1 M $LiPF_6$ in FEC/DMC electrolyte. e) The initial (dis)charge profiles of pristine Li_2CoPO_4F and Li_2CoPO_4F coated with various amounts of ZrO_2 when cycled between 2 and 5.1 V versus Li^+/Li at 10 mA g^{-1}. f) Li migration system in Li_2CoPO_4F as obtained from DFT-NEB analysis. a) Reproduced with permission.[108] Copyright 2016, American Chemical Society. b) Reproduced with permission.[112] Copyright 2011, Elsevier. c) Reproduced with permission.[114] Copyright 2012, Elsevier. d) Reproduced with permission.[117] Copyright 2015, American Chemical Society. e) Reproduced with permission.[118] Copyright 2013, Elsevier. f) Reproduced with permission.[120] Copyright 2017, American Chemical Society.

Li^+/Li. The discharge profile exhibited sloppy nature indicating a solid-solution type behavior. Good cyclability was observed till 20 cycles albeit with poor coulombic efficiency due to electrolyte decomposition.

Yang group came up with sol–gel synthesis of L2CPF where they managed to obtain carbon-coated nanometric particles.[114] Upon cycling between 2.0 and 5.4 V versus Li^+/Li, they obtained a capacity of 138 mAh g^{-1} at 1 C current rate. Even at 20 C rate, a discharge capacity of 119 mAh g^{-1} was observed. This excellent performance was attributed to nanosized particles and uniform carbon coating which enhanced the electrical conductivity of the material. The performance was found to be similar in 1 M $LiPF_6$ in EMS/DMS electrolyte except a slight improvement in the coulombic efficiency, which corresponds to the high stability of sulfone-based electrolytes at higher voltages. They also fabricated a full cell with $Li_4Ti_5O_{12}$ anode. When cycled between 0.5 and 3.9 V, the full cell delivered a capacity similar to half-cell with excellent power density (Figure 6c). However, poor cycling performance was observed due to high charge transfer resistance resulting from electrolyte decomposition. Until now, many other synthesis approaches have been adopted. However, structural transformation was observed in all cases when charged above 5 V leading to an irreversible capacity loss after first cycle.[100,115,116] Kobayashi et al. reported a detailed study on the structural changes happening in L2CPF.[117] They identified the use of fluoroethylene carbonate (FEC)-based electrolyte [$LiPF_6$–FEC/dimethyl carbonate (DMC) (1:4)] instead of EC-based electrolyte improved the capacity significantly (Figure 6d). It is due to reduced amount of PF_6^- anion formation and rapid protective film formation on the surface of L2CPF inhibiting the damage to PO_4- tetrahedra. It yielded a discharge capacity of 135 mAh g^{-1} corresponding to 0.94 Li intercalation into the structure. The underlying structural transformations at various (dis)charge states were analyzed using synchrotron XRD, X-ray absorption near-edge structure (XANES) and nuclear magnetic resonance (NMR) studies. It was observed that using FEC based electrolyte inhibited the irreversible structural change occurring at >4.8 V in ethylene carbonate (EC)-based electrolyte, which led to superior performance of L2CPF. However, they observed a phase change in the material during extraction of lithium. A second orthorhombic $Li_\beta CoPO_4F$ phase was produced from the pristine sample by a combination of solid-solution and two-phase reaction pathways during first charge. This phase change is reversible involving a volume expansion of 4.5%. From ^{7}Li MAS NMR spectroscopy coupled with classical molecular dynamics simulations, only one Li site was found to be active in (de)intercalation with other two sites remaining inactive.

One way to improve the electrochemical performance is by coating the surface with an oxide layer to avoid electrolyte decomposition. These oxide layers act as an inert layer between electrode and electrolyte especially in the case where HF is generated during side reactions. In this pursuit, Amaresh

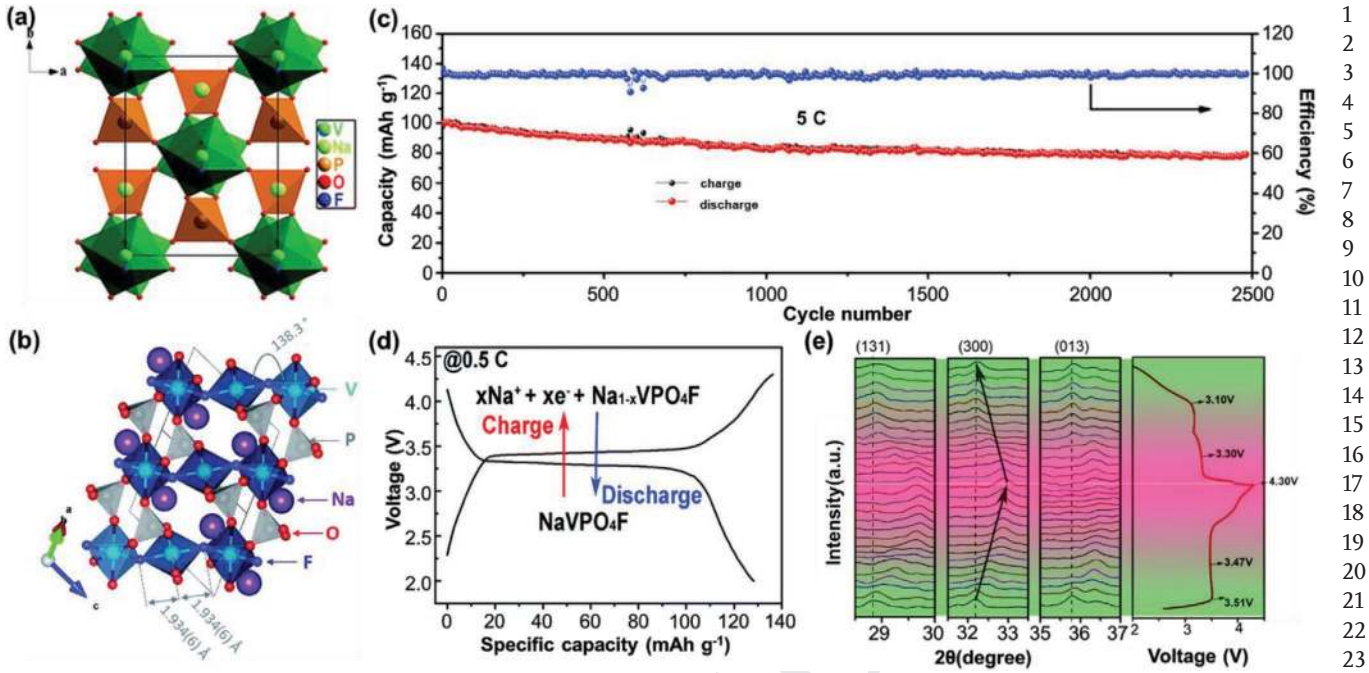

Figure 7. a) Crystal structure of monoclinic $NaVPO_4F$. b) Crystal structure of triclinic tavorite $NaVPO_4F$. c) Long-term cyclability of $NaVPO_4F$ up to 2500 cycles at 5C rate showing 70% of capacity retention at the end. d) (Dis)charge profile of monoclinic $NaVPO_4F$ at 0.5C rate when cycled between 2.0 and 4.3 V. e) In siu XRD pattern of $NaVPO_4F$ during (dis)charge. a,d,e) Reproduced with permission.[136] Copyright 2018, Royal Society of Chemistry. b) Reproduced with permission.[130] Copyright 2017, Royal Society of Chemistry. c) Reproduced with permission.[135] Copyright 2018, Elsevier.

et al. reported ZrO_2 coated L2CPF exhibiting superior performance (Figure 6e).[118] This also enhanced the active surface area favoring effective utilization of the capacity. Chang et al. were able to improve the performance by targeted nano-SiO_2 coating on the surface of L2CPF.[119] Antipov group elucidated the Li-ion transport properties in the material using theoretical approach.[120] The Voronoi–Dirichlet partitioning and BVS approaches predicted 1D pathway along [010] axis, however, density functional theory revealed additional low energy transitions indicating presence of 3D pathways (Figure 6f). They also predicted the possibility of only one Li (de)insertion in the stable operating voltage window of existing commercial electrolytes.

Exploring Mn chemistry, Li_2MnPO_4F (L2MPF) was obtained by ion exchange from Na_2MnPO_4F. It was found to be isostructural to the parent phase.[121] 2D Li-diffusion pathways were predicted using BVS calculation. It exhibited a discharge capacity of 140 mAh g^{-1} at an average cell potential of 3.9 V versus Li/Li^+. Ni-based fluorophosphate, Li_2NiPO_4F (L2NPF) was first reported in 1999 without any electrochemical activity due to decomposition of commercial electrolytes at high voltages.[122] Several attempts have been reported in literature to enhance the electrolyte voltage stability window beyond 5.5 V. Glutaronitrile or adiponitrile-based solvents were found to be stable till 8.0 V versus Li/Li^+ for electrochemical double-layer capacitors.[123] Abu-Lebdeh proposed that addition of EC as a cosolvent to adiponitrile or glutaronitrile-based solvent to enhance the stability window to 6.0 V for LIBs.[124,125] Addition of EC cosolvent to dinitrile solvent reduces the viscosity of the electrolyte and enhances the conductivity. However, aluminium corrosion is observed at such high voltages using dinitrile-based electrolytes. Okada group employed 1 M $LiBF_4$ in EC/DMC/sebaconitrile (25:25:50 by vol%) electrolyte, which is stable up to 6 V versus Li/Li^+.[126] Utilizing this electrolyte, Li_2NiPO_4F was shown to work as a 5.3 V battery cathode material for the first time. Employing classical atomistic simulation, 3D Li-ion conducting pathways were predicted along with occurrence of Li/Ni antisite defects.[127]

3.2. Fluorophosphates for Sodium-Ion Batteries

3.2.1. Vanadium-Based Fluorophosphates

$NaVPO_4F$ (NVPF) is known to exist in two polymorphs: a high temperature tetragonal phase and a low-temperature monoclinic phase. The tetragonal phase is isostructural with $Na_3Al_2(PO_4)_3F_2$ with an *I*4/*mmm* symmetry.[54] It has a 3D structure built from $[VO_4F_2]$ octahedra connected with $[PO_4]$ tetrahedra rendering open channels where Na^+ ions are located. Barker et al. first reported the tetragonal NVPF phase in 2003 synthesized via solid state route.[52] They fabricated a full-cell using hard carbon as anode delivering a discharge capacity of 82 mAh g^{-1} at an average cell voltage of 3.7 V (vs Na/Na^+) involving V^{4+}/V^{3+} redox activity. A two-step (dis)charge profile was observed.

The monoclinic polymorph of NVPF (with *C*2/*c* symmetry) was proposed by Zhuo et al. and Liu et al. (**Figure 7**a).[128,129] However, its detail structural analysis still remains an open issue. Boivin et al. reported a tavorite based $NaVPO_4F$ in which they observed the oxidation state of vanadium to be slightly higher than V^{3+} (Figure 7b). However, they could extract only

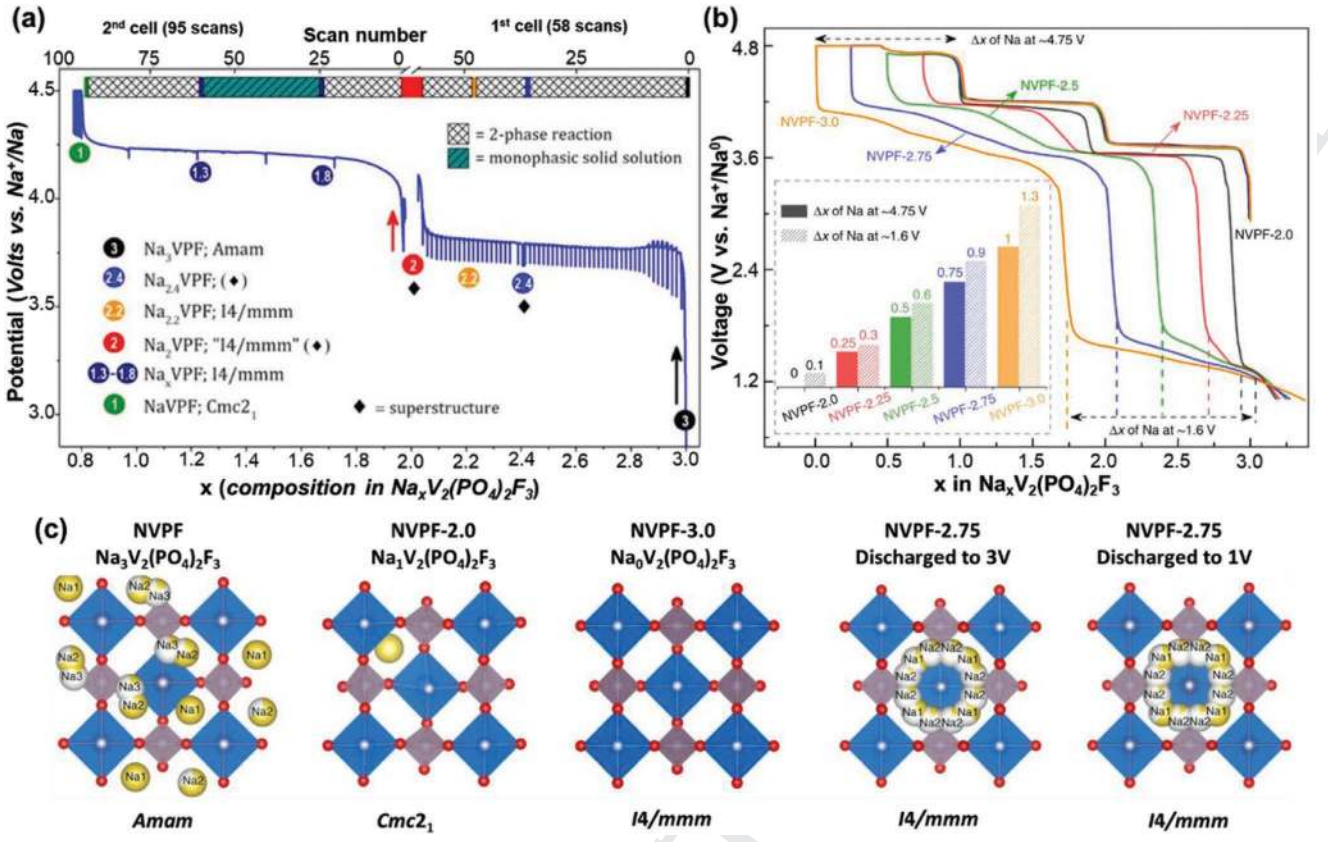

Figure 8. a) Potential versus composition curves of Na3VPF where the first cell was cycled (galvanostatic intermittent titration technique) between Na3VPF and Na2VPF and the second one is galvanostatic cycling between Na2VPF and Na1VPF. The single-phase compositions are highlighted by colored circles. b) First cycle activation of Na3VPF in which it is charged up to 4.8 V and then the charge is controlled by limiting Δx(Na) = 2, 2.25, 2.5, 2.75, 3.0 extracted followed by discharge till 1 V at C/10 rate. c) Crystal structures of NaxVPF at different states of charge. a) Reproduced with permission.[158] Copyright 2019, Wiley-VCH. b,c) Reproduced with permission.[152] Copyright 2019, Nature.

15% sodium out of the structure.[130] Many synthesis techniques have been adopted to synthesize NVPF.[20,52,131–134] Balaya group synthesized monoclinic NVPF using soft template method using V_2O_3 and V_2O_5 as precursor. NVPF synthesized by utilizing V_2O_5 as precursor delivered a discharge capacity of 121 mAh g^{-1} at 1 C current rate with a discharge plateau at 3.33 V. It delivered excellent cyclability retaining 81% of discharge capacity at the end of 10 000 cycles running at 10 C rate. Negligible volumetric changes were observed by ex situ field emission scanning electron microscopy (FESEM). This material suffers from low electronic conductivity that can be improved by carbon coating to obtain superior electrochemical performance. Feng et al. reported a bottom-up synthesis route based on hydrogen bonds to synthesize NVPF/C cathode material. The resulting nano-sized 3D coral-like structures exhibited excellent rate capability and cycling stability. A capacity of 88 mAh g^{-1} was obtained at 50 C rate, with 70% capacity retention after 2500 cycles at 5 C rate (Figure 7c).[135] Monoclinic NVPF@C prepared by molten-state-blending technique showed high crystallinity, high thermal stability and good electron/Na^+ transport. When cycled between 2 and 4.3 V, discharge capacity of ≈130 mAh g^{-1} was obtained at 0.5 C rate with a voltage plateau at 3.4 V (Figure 7d). The reversible structural change during (de) intercalation was examined using in situ XRD study (Figure 7e). A discharge capacity of 112.1 mAh g^{-1} was obtained at 30 C rate with super stable cycling performance for 1500 cycles at 20 C rate with capacity fading of just 0.0064% per cycle.[136] Recently Ge et al. reported a carbon-coated monoclinic NVPF with enhanced conductivity of 4.2×10^{-2} S cm^{-1} delivering superior cycling performance.[137] On another note, small amount of metal-ion (Cr^{3+}, Al^{3+}) doping into the V sites have been shown to improve the cyclability of monoclinic NVPF phase.[131]

NASICON structured $Na_3V_2(PO_4)_2F_3$ (N3VPF) is a widely explored vanadium based fluorophosphate owing to its high theoretical capacity involving three electron transfer reaction. Its theoretical energy density (507 Wh kg^{-1}) is comparable to commercial $LiFePO_4$.[138] Isostructural to $Na_3Fe_2(PO_4)_2(OH)_2F$ and $Na_3V_2(PO_4)_2O_2F$, the crystal structure of N3VPF was first reported by Meins et al.[54,139] It assumes a tetragonal framework (s.g. $P4_2/mnm$) consisting of $[V_2O_8F_3]$ bioctahedra units abridged by PO_4 tetrahedra units building a 3D network with Na^+ diffusion pathways along (110) and (100) directions. The PO_4-group imparts structural and thermal stability decreasing the chances of O_2 evolution thereby improving the capacity retention.[140–142] Masquelier group also carried out structural investigation using high-resolution diffraction study and observed significant orthorhombic distortion in the structure having a strong impact on the sodium distribution in

the planes.[143] Broux et. al. studied the temperature dependence of structural properties of N3VPF leading to the formation of more symmetrical tetragonal structure and complete disorder on the sodium sites.[144] They observed order-disorder transition at 125 °C, which affects the ionic properties of the material by decreasing the activation energy barrier. The electrochemical properties of N3VPF was first reported by Barker group in 2006 where they tested it as a positive electrode material for LIBs yielding a capacity of 120 mAh g^{-1}.[22,145] Shakoor et al. first demonstrated reversible Na-ion intercalation in this material.[146] However, the (dis)charge profile was contrary to Li-intercalation and exhibited two voltage plateaus at 3.7 and 4.2 V. The underlying structural changes in N3VPF are widely investigated using variety of characterization techniques.[147–149] Bianchini et. al. used high angular resolution synchrotron diffraction to unravel four different phases (**Figure 8**a).[149] Interestingly, only one of these phases was found to exhibit solid-solution process in the range of $x = 1.8–1.3$ during deintercalation, while the completely discharged product was found to have $Cmc2_1$ symmetry. They studied the symmetry differences in between these phases by resolving weak Bragg reflections. They also examined the crystal structure using direct operando measurements for the first time. Masquelier group also carried out operando X-ray absorption spectroscopy and ^{51}V solid-state NMR studies showing V^{IV} disproportionation.[150] Using vanadium K-edge XANES study, they showed the phenomenon of disproportionation occurs immediately after the extraction of one sodium-ion and not only at the end of charge. The structural changes were further studied using ^{23}Na and ^{31}P solid-state NMR studies.[148] It identified V^{4+} defects in the structure leading to increase in the Na mobility during charge process. Assuming 3 electron transfer, N3VPF can deliver a theoretical discharge capacity of 256 mAh g^{-1} but only capacity corresponding to one electron transfer can be practically realized. Electrochemically inactive Ga^{3+} ions were doped in the V^{3+} sites in order to identify whether the overall capacity is limited due to V site.[151] $Na_3GaV(PO_4)_2F_3$ delivered a capacity of 141 mAh g^{-1} indicating that $Na_3GaV(PO_4)_2F_3$ is site-limited and not redox-limited. Constant efforts have been made to enhance the energy density of the material to inch closer to commercialization with performance comparable to existing lithium cathodes. One such possible route is by activating the third sodium ion present in the structure. However, this process is not trivial since it is theoretically predicted that the third sodium ion can be removed from the structure at >4 .9 V versus Na/Na^+, which is too high for the existing electrolytes. However, Tarascon group recently demonstrated the removal of third sodium ion from the pristine structure during charge leading to formation of a disordered phase of tetragonal symmetry capable of intaking three sodium ions during subsequent discharge when cycled in voltage range of 1–4.8 V with the last sodium ion being inserted at 1.6 V (vs Na/Na^+) (Figure 8b).[152] It remains disordered upon cycling. They also studied the distribution of sodium inside the crystal structure of N3VPF at various states of charge by recording ex situ X-ray diffraction patterns (Figure 8c). A full cell was also fabricated using disordered N3VPF showing an increase in energy density by 10–20%. The electrochemical performance of the material is limited by low intrinsic electrical conductivity and large particle size, that can be improved by carbon-coating, particle downsizing and/or alkali/metal-ion doping.[153–156] Carbon coating enhances the electronic conductivity, smaller particle size implies shorter diffusion length hence improving the performance at higher C rates, while metal/alkali ion doping broadens the diffusion pathway inside the structure. Carbon-coated N3VPF delivered a discharge capacity of 130 mAh g^{-1} with good cycling stability up to 3000 cycles. N3VPF@C/CNT composite synthesized via spray drying technique showed a discharge capacity of 85 mAh g^{-1} even at a fast current rate of 30 C. High tap density was obtained from N3VPF/C@RGO composites. Moderate substitution of potassium in some vanadium sites led to broadened ion diffusion pathways, hence improving the overall electrochemical performance. It delivered superior electrochemical performance than pristine N3VPF and N3VPF@CNT composite. A capacity of 120 mAh g^{-1} was achieved at 1 C rate and over 90 mAh g^{-1} was achieved at 10 C rate after 1600 cycles.[157] Even at 50 C, the cell was able to retain 90% of the capacity after 6000 cycles. Broux et al. recently assembled 18650 prototype cells using N3VPF as cathode and hard carbon anode delivering an energy density of 75 Wh kg^{-1} with excellent cyclability and rate capability. The carbon-coated N3VPF showed good electrochemical performance even at 0 °C. [158] Nguyen et al. reported the solid solution between $Na_3V_2(PO_4)_2F_3$ and $Na_3V_2(PO_4)_2FO_2$.[159] The solid solution was further studied by density functional theory method and ^{31}P and ^{23}Na magic-angle spinning NMR study.[160] They observed complex spin transfer mechanism between the two materials because of the peculiar nature of electronic structure of V-ions.

The $Na_3(VO_{1-x}PO_4)_2F_{1+2x}$ $(0 \le x \le 1)$ (N3VOPF) family of vanadium fluorophosphates involving both V^{4+}/V^{3+} oxidation states can be obtained by oxygenation of N3VPF. In this family, $Na_3(VO)_2(PO_4)_2F$ (N3VOPF) has a theoretical capacity of 130 mAh g^{-1} with high energy density. First reported by Sauvage et al. and Massa et al., it crystallizes in tetrahedral structure with $I4/mnm$ space group.[161,162] Tsirlin et al. reported a different room temperature polymorph with $P4_2/mnm$ space group as shown in **Figure 9**a.[163] Both N3VPF and N3VOPF exhibit similar structures with replacement of one of the F-atom by O-atom. Sauvage et al. were the first to study the electrochemical activity in this system, reporting a discharge capacity of 87 mAh g^{-1} at C/100 rate having with two voltage plateaus at 3.6 and 4.0 V (vs Na/Na^+).[161] $Na_3(VO_{1-brx}PO_4)_2F_{1+2x}$ family was reported by Rojo group in 2012.[164] N3VOPF with mixed V^{4+}/V^{3+} valence state was demonstrated by Park et al. and Qi et al.[165,166] $Na_3V_2O_2(PO_4)_2F$ prepared by solvothermal route delivered a discharge capacity of 73 mAh g^{-1} at 10 C rate along with 90% of capacity retention at 2 C rate for 1200 cycles.[165] Mono crystalline 3D nanostructured N3VOPF formed on flexible graphene exhibited superior rate capability delivering a discharge capacity of 45 mAh g^{-1} even at 60 C rate (Figure 9b).[167] This performance was attributed to low in-plane energy barrier, fast ion transport within *ab*-plane and minimal volumetric change during (de)intercalation. The structural evolution during cycling was studied by various groups and both solid-solution and two-phase reaction were observed.[168–170] Redox transitions and relationship between V^{4+}/V^{3+} and V^{5+}/V^{4+} redox reactions along with Na^+ intercalation mechanism during charge storage process were studied by Park et al. The energy density of N3VOPF

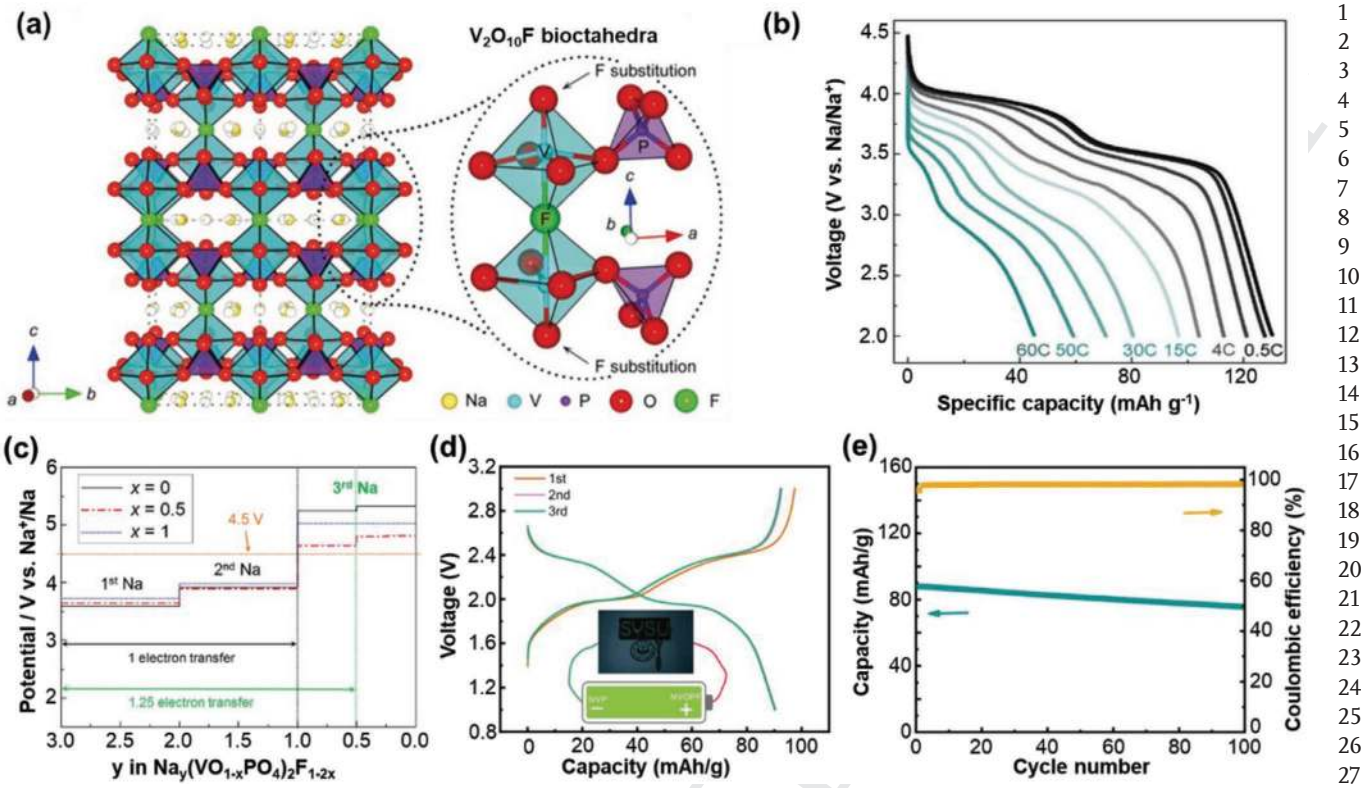

Figure 9. a) Crystal structure of Na_3VOPF with $P4_2/mnm$ space group. b) Rate capability of Na_3VOPF at different C-rates. c) Theoretical calculations showing potential corresponding to three different Na-deintercalation from Na_3VOPF. d,e) (Dis)charge profile of $Na_3VOPF||Na_3V_2(PO_4)_3$ full cell cycled at 10 C rate delivering a discharge capacity of 91 mAh g^{-1}. The cyclability of the full cell up to 100 cycles showing 86% capacity retention at the end. a) Reproduced with permission.[165] Copyright 2012, Nature. b) Reproduced with permission.[166] Copyright 2018, Wiley-VCH. c) Reproduced with permission.[170] Copyright 2014, Wiley-VCH. d,e) Reproduced with permission.[183] Copyright 2019, Wiley-VCH.

can be further increased if the third Na-ion can also be extracted out of the system. But it is restricted due to high operating voltage of 5.3 V Na/Na^+ (Figure 9c). However, theoretical calculations predicted replacing O with Cl to form $Na_3V_2Cl_2(PO_4)_2F$ can increase the energy density to 758 mAh g^{-1}.[171] N3VOPF also suffers from low intrinsic electronic conductivity that can be circumvented by modifying the synthesis technique, carbon coating, particle nanosizing and by adding various additives.[172–178] Carbon-coated N3VOPF delivered a discharge capacity of 68 mAh g^{-1} at 1 C rate.[173] N3VOPF/rGO composite exhibited a discharge capacity of 120 mAh g^{-1} at C/20 rate and 91.4% capacity was retained after 200 cycle at C/10 rate.[172] Jin et al. reported 3D N3VOPF@C/graphene composite delivering a capacity of 136 mAh g^{-1}.[179] RuO_2 coated N3VOPF nanowires provided long term cycling stability up to 1000 cycles and a high rate capability with 95 mAh g^{-1} at 20 C rate.[180] Full cell with hard carbon anode delivered a specific capacity of 120 mAh g^{-1} at a working voltage of 3.1 V. [181] Recently carbon encapsulated N3VOPF was synthesized by rapid microwave-assisted technique and delivered a capacity of 127.9 mAh g^{-1} with 82.1% retention after 2000 cycles at 20 C rate.[182] It also led to good rate kinetics and cycling performances of N3VOPF in lithium half-cell configuration. Zhang et al. fabricated a full-cell with Na_3VOPF/rGO composite cathode and $Na_3V_2(PO_4)_3$ anode and it delivered a capacity of 91 mAh g^{-1} at 10 C rate with 86% retention after 100 cycles as shown in Figure 9d,e.[183] A specific capacity of 79 mAh g^{-1} was obtained at 60 C rate with the full cell and remains the best rate capability reported in literature till date. Overall, vanadium-based fluorophosphates form a rich family of sodium insertion materials with structural diversity, chemical/thermal stability, efficient electrochemical activity, and potential practical applications.

3.2.2. Fluorophosphates with General Formula Na_2MPO_4F (M = Fe, Co, Mn, Ni)

Exploring fluorophosphate chemistry, Nazar group reported Na_2FePO_4F (NFPF) as a multifunctional cathode material in 2007.[18] It has an orthorhombic structure (s.g. *Pbcn*) built from FeO_4F_2 octahedra, which are face-shared to form $Fe_2O_7F_2$ bioctahedra units. These bioctahedra units are connected by bridging F-atom to form chains, which are interconnected by PO_4-group to form $[FePO_4F]$ slabs. Na-atoms are present in two different crystallographic sites facilitating 2D diffusion pathways. When tested for its (de)intercalating properties in Li-ion half-cell configuration, a discharge capacity of 115 mAh g^{-1} was obtained at an average cell potential of 3.5 V (vs Li/Li^+). The (dis)charge profiles exhibited a sloppy nature suggesting the presence of quasi solid-solution behavior. It exhibits one electron redox activity with no possibility to extract the second Na ion due to the high potential and structural instability associated with

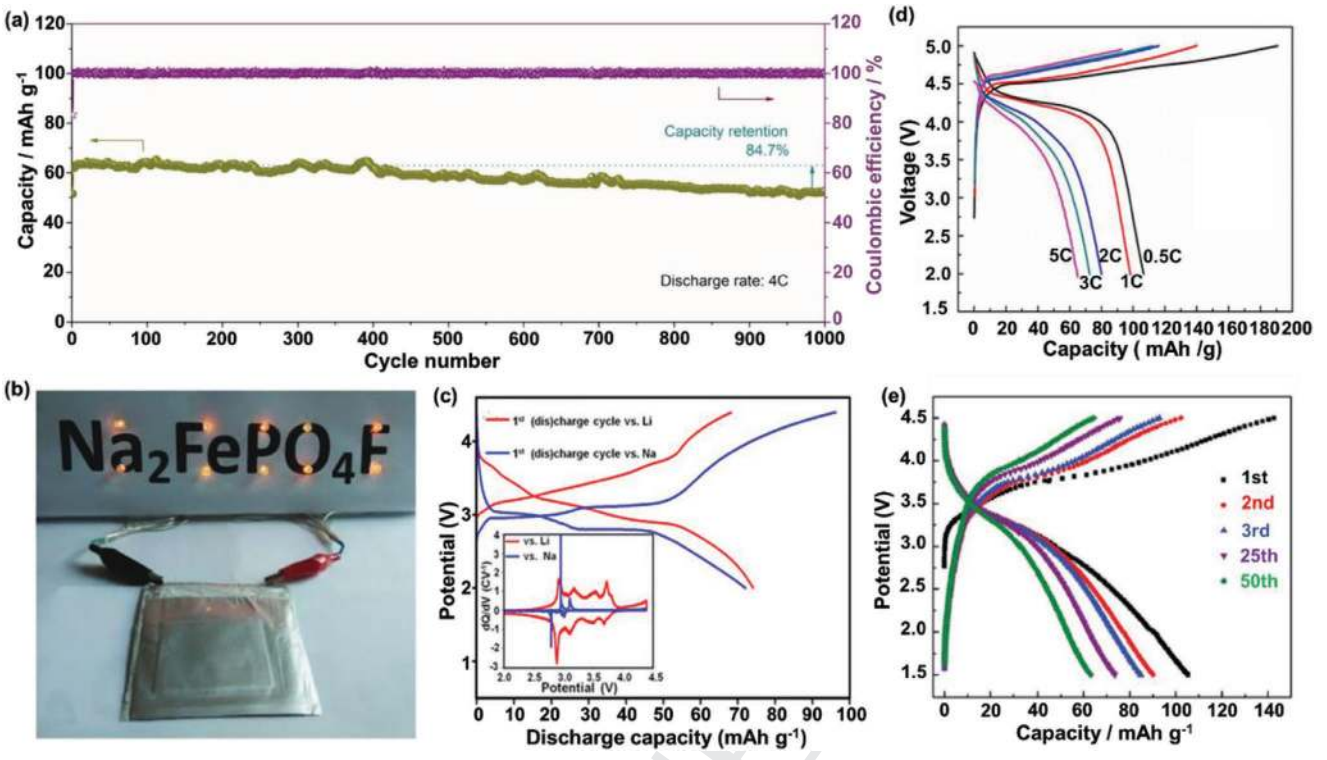

Figure 10. a) Cyclability of Na_2FePO_4F/C at 4 C rate for 1000 cycles showing 84.7% capacity retention at the end. b) Picture of the pouch cell assembled using Na_2FePO_4F@C nanofibers cathode and carbon nanofibers anode. c) Different nature of (dis)charge profiles of NFPF when cycled in lithium half-cell configuration and sodium half-cell configuration. (Inset) dQ/dV plots of Na_2FePO_4F (dis)charge profiles. d) Rate capability of Na_2CoPO_4F at various cycling rates. e) The (dis)charge profile of Na_2MnPO_4F cycled between 1.5 and 4.5 V at 6.2 mA g^{-1} up to 50 cycles. a) Reproduced with permission.[192] Copyright 2017, American Chemical Society. b) Reproduced with permission.[197] Copyright 2019, Wiley-VCH. d) Reproduced with permission.[207] Copyright 2015, The Electrochemical Society. e) Reproduced with permission.[208] Copyright 2014, Royal Society of Chemistry.

Fe^{4+}/Fe^{3+} redox activity. Recham et al. first tested the ionothermally synthesized NFPF for Na-intercalation.[19] The nanoscale particles showed efficient Na-(de)intercalation leading to a first discharge capacity of 120 mAh g^{-1} (Q_{Th} = 124 mAh g^{-1}) at 3.0 V (vs Na/Na^+).

It has been observed that the particle size and morphology plays a key role in the electrochemistry of cathode materials, hence many synthesis methods for NFPF have been reported till date.[184–195] Deng et al. reported a green route based synthesis technique where Vitamin C was used as a carbon source to yield Na_2FePO_4F/C.[192] They reported 84.7% of capacity retention at 4 C rate after 1000 cycles as shown in **Figure 10**a. NFPF is a poor electrical conductor, thus warranting carbon coating to improve the electrochemical performance. Komaba group first demonstrated the positive effect of carbon coating of NFPF by adding citric acid. Sharma et al. reported an economic combustion synthesis route to obtain carbon coated nanoparticles with porous morphology using Fe(III) based precursor. They reported a discharge capacity over 100 mAh g^{-1} at 3.0 V (vs Na/Na^+). rGO-coated NFPF was found to deliver a discharge capacity of 60 mAh g^{-1} at 1 C current rate and 70% of it was retained at the end of 5000 cycles. Jin et al. used DFT calculations to find out optimum dopants to improve the intrinsic electrical conductivity of the material.[196] They observed Co-doped NFPF as the most promising candidate. The $Na_2Fe_{0.94}Co_{0.06}PO_4F$/C delivered a capacity of 99.93 mAh g^{-1} at 0.2 C and observed a capacity retention of 62% after 400 cycles at 1 C current rate. Wang et al. synthesized nanometric NFPF particles embedded in porous N-doped carbon nanofibers to obtain a high reversible capacity of 117.8 mAh g^{-1} at 0.1 C rate with excellent cycling stability up to 2000 cycles.[197] Pouch cells were assembled using NFPF@C nanofibers cathode and carbon nanofibers anode to deliver an energy density of 135.8 Wh kg^{-1} (Figure 10b).

However, the (dis)charge profile during Li-and Na- intercalation is different indicating different underlying structural transitions (Figure 10c).[198] During lithium (de)intercalation, a sloppy profile is observed while in case of sodium two distinct plateaus are observed. The small size of Li^+ cation leads to random occupancy of the Na1 and Na2 sites during intercalation implying no specific ordering of Li in the structure. Whereas, the two different site energies related to two crystallographic sites Na1 and Na2 lead to different intercalating voltage. Nevertheless, the structural transition is worth studying in both cases. Smiley et al. employed ex situ ^{23}Na solid-state NMR spectroscopy to probe the ion mobility during cycling.[199] From NMR study, they proposed a biphasic extraction process of Na-ions from the structure. However, no intermediate phase was detected with coexistence of Na_2FePO_4F and $NaFePO_4F$ end phases. The role of semilabile oxygen, i.e., the oxygen linked only to P and alkali atoms was studied by Abakumov group.[200] They observed an identical coordination environment for both sites of sodium and proposed different intercalating behavior

due to different number of bonds to the semilabile oxygen atoms. The site having large cation-semilabile oxygen interaction is characterized by higher deintercalation potential while the sites with low interaction exhibits lower potential. They observed a solid-solution mechanism during delithiation while an intermediate monoclinic phase $Na_{1.5}FePO_4F$ ($P2_1/b$) was observed during desodiation. Fe(II)/Fe(III) charge ordering along with Na vacancy ordering was also observed. Yang group combined ex situ experiments with theoretical calculations to further analyze the structural changes in the material during cycling.[201] They found the cycling process is dominated by two biphasic reactions during various states of charge keeping the sodium in Na1 site intact. The structure of intermediate phase $Na_{1.5}FePO_4F$ was indexed to monoclinic structure (s.g. $P2_1/c$) with the help of DFT calculations and ex situ ^{23}Na NMR studies. Yamashita group employed first principle calculation along with Monte Carlo method to analyze the (dis)charge mechanism of NFPF.[202] They found the most stable structure of $Na_{1.5}FePO_4F$ having monoclinic structure (s.g. $P2_1/b11$). Indeed, structural evolution during (de)insertion in Na_2FePO_4F still remains vague warranting further research. While the extraction of second sodium ion is difficult, Wu et al. reported a 1.46 electron transfer per formula unit at 60 °C when cycled between 1.5 and 4.6 V in Li-cell.[203] Avdeev et al. studied the magnetic structure of NFPF observing a long-range antiferromagnetic ordering transition at 3.4 K.[204]

The isostructural Co-analog, Na_2CoPO_4F (NCPF) was reported by Nazar group in 2010.[205] Following, Komaba group reported its first electrochemical report in 2014.[206] The solid-state synthesized material was reported as a high-voltage (≈4.4 V vs Na/Na^+) sodium battery cathode with a discharge capacity of 71 mAh g^{-1}. The large irreversible capacity loss during first cycle was attributed to decomposition of electrolytes at higher voltages as shown in Figure 10d.[195] Later, Yang group came up with spray drying synthesis technique to form NCPF with spherical morphology yielding a discharge capacity of 107 mAh g^{-1} at an average cell voltage of 4.5 V albeit with large capacity fading.[207]

Deviating from orthorhombic Na_2FePO_4F and Na_2CoPO_4F, Na_2MnPO_4F (NMPF) assumes a monoclinic framework with $P2_1/n$ symmetry. It consists of corner shared MnO_4F_2 octahedra connected by F-atoms to form $Mn_2O_8F_2$ bioctahedra chains, which are abridged by PO_4 tetrahedra giving rise to a 3D structure. Despite having open pathway for Na^+ diffusion, NMPF was found to be electrochemically inactive.[19,205] Wu et al. synthesized carbon coated NMPF and reported a discharge capacity of 98 mAh g^{-1} at 60 °C, but with poor cyclability.[203] The diffusion kinetics and electrochemical activity was analyzed by Kim et al. by combining experiments results with DFT calculations.[121] In the solid-state synthesized sample, the Na^+ diffusion is along b-direction. They also synthesized Li_2MnPO_4F by ion-exchange method exhibiting superior electrochemical activity, which was attributed to an additional diffusion pathway perpendicular to F^- backbone. Enhanced electrochemical performance was obtained with a discharge capacity of 110 mAh g^{-1} by carbon-coated NMPF hollow spheres synthesized via spray drying route (Figure 10e).[208] The material was found to be structurally stable even at higher voltages. Na_2NiPO_4F (NNPF) has been synthesized without any report on electrochemical study as it is active >5 V, where the conventional electrolytes start to decompose.[205] Overall, this class of material is very attractive in terms of realizing high voltage cathode materials for Na-ion batteries. Especially Na_2FePO_4F form an economic sodium insertion material with moderate energy density suitable for stationary applications.

3.2.3. Fluorophosphates in Aqueous Batteries

Fluorophosphate based insertion materials can also be implemented in aqueous systems. Aqueous batteries enhance the ionic conductivity and impart operational safety. Care must be taken to avoid water splitting beyond the narrow safe operating voltage window. Consequently, not all high voltage materials can be tested in aqueous electrolytes. However, suitable additives and highly concentrated electrolytes broaden the working voltage window making it possible to test high-voltage cathode materials in aqueous media. NASICON type $NaVPO_4F$ was the first fluorophosphate to be tested in aqueous electrolytes. It delivered a discharge capacity of 54 mAh g^{-1} in 5 M $NaNO_3$ solution with two plateaus at 0.8 and 0.2 V (vs SCE).[209] Kumar et al. reported electrochemical properties of $Na_3V_2O_2(PO_4)_2F$-multiwall carbon nanotubes (MWCNT) nanocomposites in aqueous electrolyte, delivering a discharge capacity of 35 mAh g^{-1} at 1 C rate in half-cell configuration.[175] The $Na_3V_2O_2(PO_4)_2F$ -MWCNT || $NaTi_2(PO_4)_3$-MWCNT full cell gave a discharge capacity of 42 mAh g^{-1} at 1 C rate. Recently, Sharma et al. tested Na_2FePO_4F (NFPF) by employing 17 M $NaClO_4$ aqueous electrolyte.[210] Using this supersaturated electrolyte, the operating voltage window can be enlarged to 2.8 V in 17 M $NaClO_4$ vis-a-vis 1.23 V in conventional water-based electrolytes.[211] The NFPF half-cell delivered a reversible discharge capacity of 84 mAh g^{-1} when cycled in an optimized voltage range of –0.9 to 0.9 V versus Ag/AgCl reference electrode at 1 mA cm^{-2} current density as shown in **Figure 11**a. It exhibited good cycling stability and rate kinetics. A full-cell was also assembled with NASICON-type $NaTi_2(PO_4)_3$ anode giving a specific capacity of 85 mAh g^{-1} at an average cell potential of 0.7 V (Figure 11b). Recently, $Na_3V_2(PO_4)_2F_3$-single walled carbon nanotubes (SWCNT) composites were also tested in 17 M $NaClO_4$ electrolyte.[212] The half-cell configuration delivered a discharge capacity of 81.3 mAh g^{-1} but with poor coulombic efficiency due to the formation of solid-state interface (SEI) (Figure 11c). The $Na_3V_2(PO_4)_2F_3$-SWCNT || $NaTi_2(PO_4)_3$-MWCNT full cell delivered an energy density of 150 Wh kg^{-1} at 1.92 V in the voltage range of 0.6–2.1 V (Figure 11d). It is possible to exploit many fluorophosphate insertion compounds in aqueous batteries with appropriate optimization of electrolytes, stabilizing additives and voltage operation window.

3.3. Fluorophosphates for Potassium-Ion Batteries

Graphite, being a standard anode for Li-ion batteries, does not serve the same purpose for Na-ion batteries as Na^+ (de)insertion is energetically not favorable in graphitic domains. Hence, hard carbon is utilized as an anode for SIBs. However, hard carbon delivers poorer performance than graphite, reducing the overall energy density by 20% as compared to LIBs. In contrast,

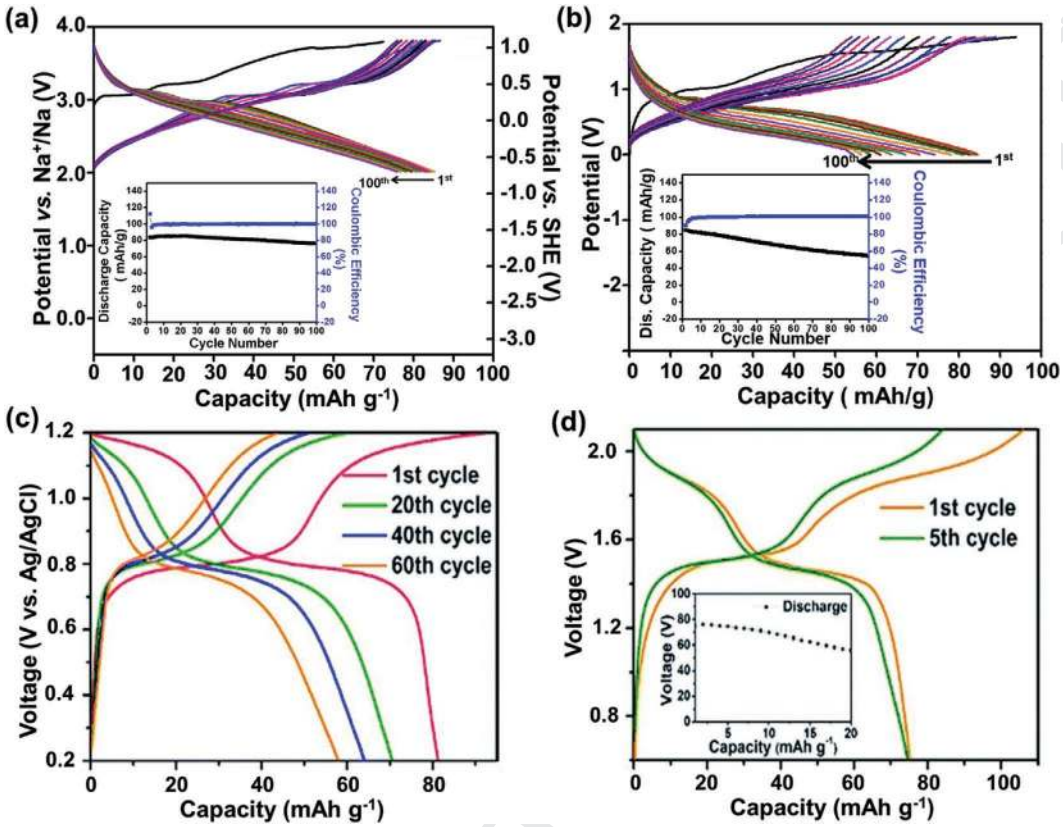

Figure 11. a) The (dis)charge profile of NFPF in hall cell configuration using 17 M $NaClO_4$ as aqueous electrolyte in the voltage range of –0.9 to 0.9 V versus Ag/AgCl. (Inset) Cyclability of half-cell up to 100 cycles. b) The (dis)charge profile of NFPF || $NaTi_2(PO_4)_3$ full-cell using 17 M $NaClO_4$ as an electrolyte. (Inset) Cyclability of full-cell up to 100 cycles. c) The (dis)charge profile of Na3VPF-SWCNT in hall-cell configuration using 17 M $NaClO_4$ aqueous electrolyte. d) The (dis)charge profile of Na3VPF-SWCNT || $NaTi_2(PO_4)_3$-MWCNT full-cell using 17 M $NaClO_4$ electrolyte. c,d) Reproduced with permission.[212] Copyright 2019, Royal Society of Chemistry.

a facile potassium (de)insertion is feasible in graphite.[213] This, coupled with its lower standard redox potential than sodium and high elemental abundance, has ushered scientific interest to develop potassium-ion batteries (KIBs).[214] The large ionic size of potassium creates a bottleneck in terms of designing appropriate host materials. Many oxide-based materials have been studied for their potassium (de)intercalating properties.[215–220] However, Tarascon group first utilized the fluorine chemistry when they reported $KFeSO_4F$ similar to $KTiOPO_4$ (KTP) structure.[221] On a similar note, Antipov group unveiled $KVPO_4F$ (KVPF) in 2016 adopting KTP structure, tested for Li (de)insertion.[222] It consists of helical chains of VO_4F_2 octahedra and PO_4 tetrahedra giving rise to a rigid framework with 3D pathways for K-ion diffusion. KVPF was first oxidized until 4.8 V in a potassium based half-cell, where it was kept under hold for 5 h at constant voltage to obtain $K_{0.15}VPO_4F$ phase. This electrode, when cycled in a lithium half-cell between 2 and 4.7 V, was found to intercalate 0.7 Li ion per formula unit at an average cell voltage of 4 V (vs Li/Li^+). The lithiated material was found to have *Pnma* space group in contrast to pristine KVPF having $Pna2_1$ symmetry. Involving 1D Li^+ diffusion, it exhibited electrochemical activity even at high current rates of 40 C. Komaba group demonstrated the potassium intercalation in KVPF for the first time.[223] Utilizing 0.7 M KPF_6 in EC:diethyl carbonate (DEC) as electrolyte, they cycled the material between 2.0 and 4.8 V yielding a first discharge capacity of 70 mAh g^{-1} with V^{4+}/V^{3+} redox potential centered at 4.02 V (**Figure 12**a). Despite irreversible capacity loss in the first cycle due to electrolyte decomposition at high voltage, excellent rate capability was observed with 90% capacity retention at 5 C rate. It is attributed to the lower Lewis acidity of K^+ ions as compared to Li^+ ions and the open structure of KVPF. In situ XRD measurements revealed single-phase structural evolution while charging from OCV to 4.8 V (Figure 12b). When charged till 5.0 V, a stable discharge capacity of 80 mAh g^{-1} was observed with an average redox potential of 4.13 V. When 1 M KPF_6 in EC:propylene carbonate (PC) (1:1, v:v) was used as electrolyte, minimal initial capacity loss and a discharge capacity of 92 mAh g^{-1} was observed. In contrast, Ceder group demonstrated the presence of several biphasic reactions during potassium (de)intercalation in KVPF.[214] When cycled between 3 and 5 V, four distinct plateaus were observed, which was confirmed by the differential capacity plots (Figure 12c). A capacity of 105 mAh g^{-1} at a nominal voltage of 4.33 V (vs K/K^+) was observed. They studied the structural evolution using *ex-situ* XRD and *ab-initio* calculations showing the formation of stable intermediate compounds at $x = 0.75$, 0.625, and 0.5. They also demonstrated that oxygenation of KVPF led to a more disordered structure along with disappearance of plateaus. Partial substitution of fluorine by oxygen was found to decrease the capacity and nominal voltage.

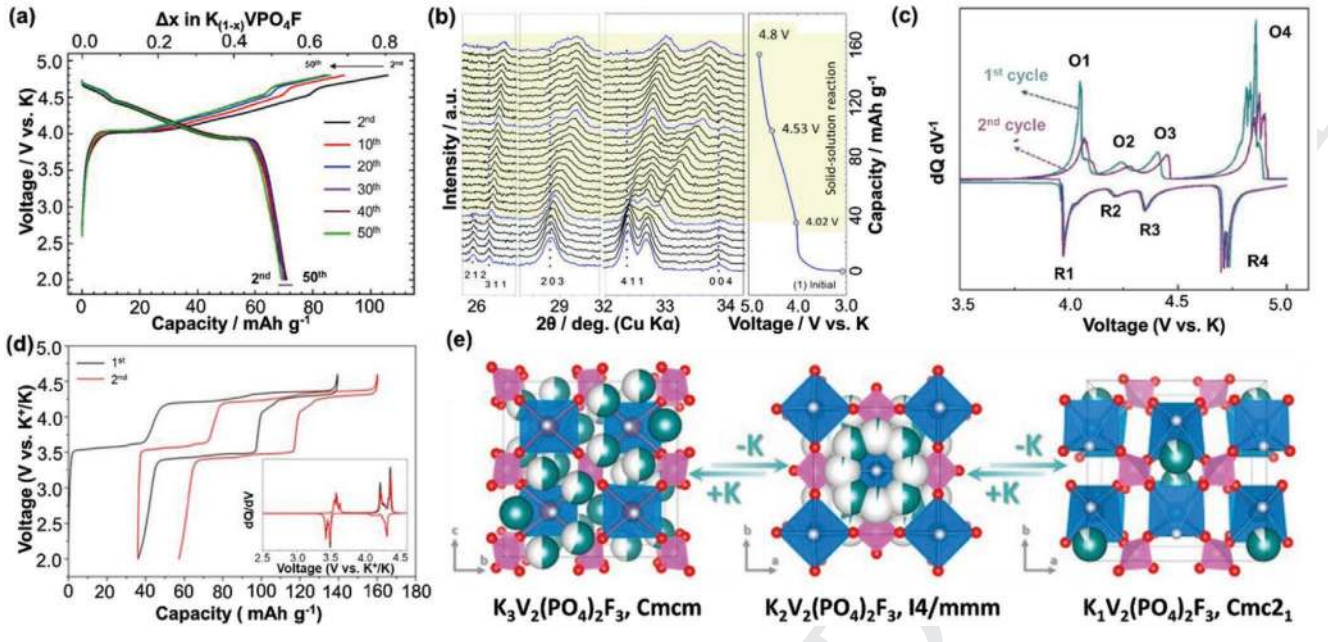

Figure 12. a) (Dis)charge profile of $KVPO_4F$ in the voltage range of 2–4.8 V (vs K/K^+). b) Operando XRD patterns of $KVPO_4F$ at C/30 rate using 0.7 M KPF_6 in EC/DEC (1:1 v/v) + 2% FEC as electrolyte. c) Differential capacity plots of $KVPO_4F$ for the first two cycles showing presence of many phases. d) Voltage profile of $K_3V_2(PO_4)_2F_3$ for the first two cycles with dQ/dV plot (inset). e) Phase transformations in $K_3V_2(PO_4)_2F_3$ during potassium (de) insertion. a,b) Reproduced with permission.[223] Copyright 2017, Royal Society of Chemistry. c) Reproduced with permission.[214] Copyright 2018, Wiley-VCH. d,e) Reproduced with permission.[213] Copyright 2019, Elsevier.

Recently, $K_3V_2(PO_4)_2F_3$ (K3VPF) phase was obtained by electrochemical ion exchange from $Na_3V_2(PO_4)_2F_3$.[213] It was found to crystallize in an orthorhombic structure with *Cmcm* space group. A potassium-based half-cell was assembled and it was charged up to 4.6 V to extract Na^+ ions. Upon progressive cycling, some structural change occurred in the material upon K intercalation leading to the switching of K^+ and Na^+ site and hence making all Na-sites accessible for (de)intercalation. The structural reorientation during subsequent cycling was also studied. On cycling between 2.0 and 4.6 V, a discharge capacity of 104 mAh g^{-1} was obtained at 3.7 V versus K^+/K at a current density of 10 mA g^{-1} (Figure 12d). Structural variation was observed in fully charged and fully discharged samples using Rietveld refinement (Figure 12e). Full cell assembled using K3VPF cathode with graphite anode showed a 3.4 V KIB activity with stable performance. The recent developments in KIBs by utilizing fluorophosphates based host materials are very promising. At this nascent juncture, a variety of fluorophosphate chemistry, particularly isostructural to Na-based compositions, can be developed for high-voltage KIBs with due optimization in structure/morphology of cathodes, binders, and electrolytes.

4. Electrocatalysis

4.1. Fluorophosphates as Electrocatalysts

Existing intercalation-based battery technologies like LIBs and SIBs are not able to cope up with the ever-growing global energy demand. In the quest to achieve high energy density storage systems, rechargeable metal–air batteries based on O_2–H_2O chemistry are widely being investigated to deliver high energy density compared to the existing state-of-the-art LIBs.[224] For example, Li–air battery can deliver an energy density up to 5200 Wh kg^{-1}. In parallel, the limited lithium-based mineral reserves, cost and safety have led to the emergence of sodium–air batteries.[225,226] These storage systems hold promise for greener energy economy relying on electrochemical water splitting. Hydrogen evolution and oxidation (HER and HOR) as well as oxygen reduction and evolution (ORR and OER) are central redox processes for hydrogen production, fuel cells and metal–air batteries. While HER/HOR occurs at E^0 = 0 V (vs RHE), ORR/OER need a catalyst to overcome the overpotential to drive the reaction (**Figure 13**a). Metal–air batteries and fuel cells work on ORR and OER processes.[227–229] Since both processes involve four-electron transfer mechanism with inherently sluggish kinetics, they require catalysts to overcome the activation barrier. This sector employs materials based on precious metals like platinum (Pt), iridium (Ir), and ruthenium (Ru). However, their practical usage is limited owing to their high cost, low abundance, stability, and the selective catalysis nature.[230] While Pt/C is the best catalyst for ORR, Ir- and Ru-based oxides catalyze OER reaction effectively. OER and ORR reactions occur during the charging and discharging of metal–air batteries. Moreover, the performance of the metal–air battery in nonaqueous (organic) electrolyte is largely affected due to the formation of insoluble discharge products, which clog the active sites on the surface of electrode so as to reduce the net efficiency. This issue can be circumvented by using aqueous hybrid metal–air battery where the discharge products are soluble.[231] Overall, these

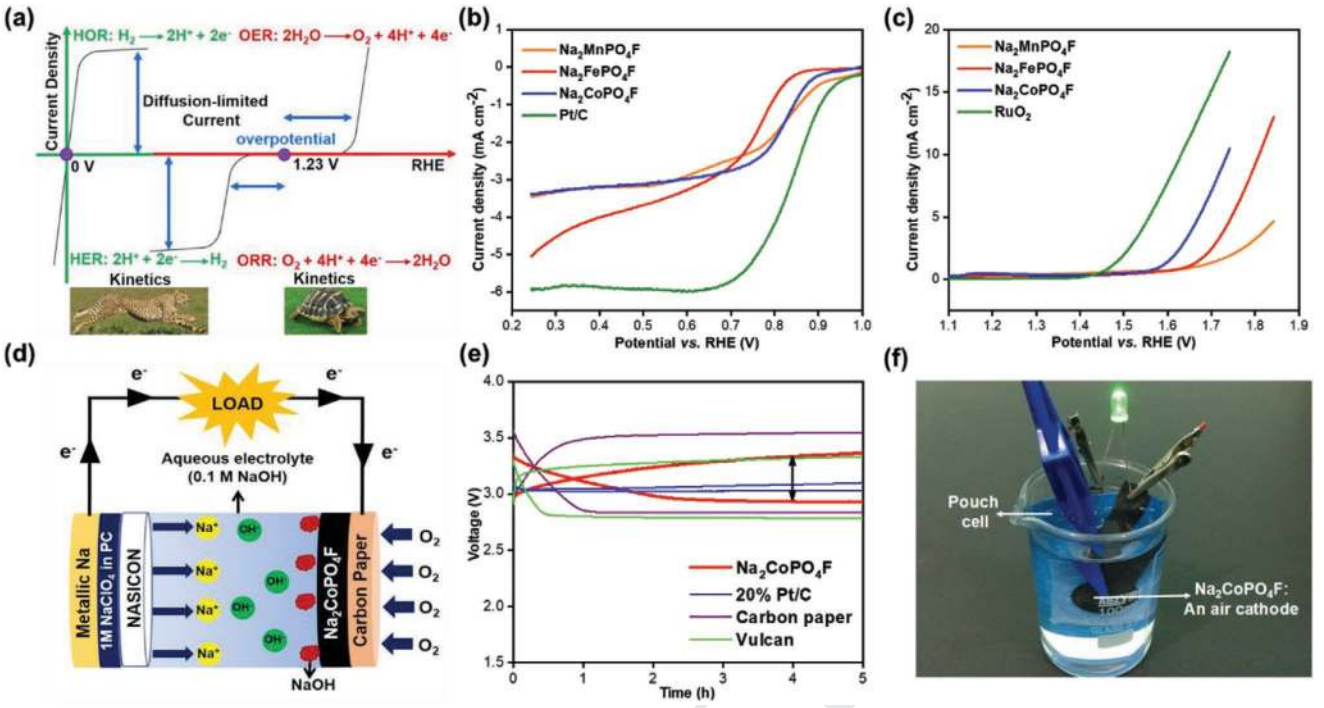

Figure 13. a) Schematic representation of polarization curves for HER/HOR and ORR/OER along with the reactions involved. Green line indicates reaction involving hydrogen while red line indicates for oxygen. b) Linear sweep voltammograms (LSV) for Na_2CoPO_4F, Na_2FePO_4F, Na_2MnPO_4F, and 20% Pt/C recorded at 1600 rpm in 0.1 M KOH electrolyte during ORR reaction. c) LSV plots of Na_2CoPO_4F, Na_2FePO_4F, Na_2MnPO_4F, and RuO_2 recorded at 1600 rpm in 0.1 M KOH electrolyte during OER reaction. d) Schematic diagram of hybrid Na–air battery. e) Comparison of NCPF as an air cathode with carbon-paper, Vulcan carbon and Pt/C. f) A practical demonstration to lit up an LED using the power withdrawn from hybrid Na–air battery utilizing the properties of Na_2CoPO_4F as an air cathode.

metal–air batteries warrant the development of economic and bifunctional air cathodes.

At this juncture, various battery insertion materials have been investigated for their electrocatalytic properties.[227–229,231–244] Notably, transition metal-based phosphate compounds have shown promising bifunctional activity along with structural stability. Some such examples are Co-based phosphate ($NaCoPO_4$), pyrophosphate ($Na_2CoP_2O_7$) and metaphosphate ($NaCoP_3O_9$). Inspired by efficient catalytic activity in these phosphates, Sharma et al. tested the electrocatalytic performance of fluorophosphate Na_2CoPO_4F (NCPF) on ring rotating disc electrode using 0.1 M NaOH alkaline solution as electrolyte.[241,245] For ORR, the CV was recorded in the range of 0.1 to −0.7 V versus Hg/HgO in an O_2 saturated electrolyte. The onset potential was found to be 0.903 V versus RHE with a current density of 3.4 mA cm^{-2}, which marks the promising ORR activity of NCPF. The stability of the material was also tested for 10 h with negligible current loss. The activity of NCPF system can be attributed to the extra structural stabilization imparted by PO_4-group and the ionic nature in the bonds due to electronegative F-atoms. Following, the OER properties were tested in the voltage range of 0.0–0.8 V versus Hg/HgO (later converted to RHE). An overpotential of 0.38 V versus RHE was observed with excellent current density. The efficient bifunctional activity in NCPF served as the motivation to test the electrocatalytic properties of whole fluorophosphate family. These fluorophosphates (Na_2MPO_4F, M = Fe/Mn/Co) were synthesized via solution combustion route leading to porous morphology and carbon coating favoring the electronic conductivity and catalytic performance. The results were benchmarked against 20% Pt–C for ORR and RuO_2 for OER. An onset potential of 0.891 and 0.909 V was recorded for Na_2FePO_4F (NFPF) and Na_2MnPO_4F (NMPF), respectively. The ORR properties of fluorophosphates were comparable to 20% Pt/C following an order of NCPF > NMPF > NFPF (Figure 13b). While all three materials exhibited promising ORR activity, very low current density was observed during OER with an overpotential of 0.49 and 0.46 V (vs RHE) for NMPF and NFPF respectively (Figure 13c). The OER activity can be attributed to the tuned energy levels of the antibonding states of M—O bonds due to F-atoms. On a broader note, these fluorophosphates were found to retain structural stability after prolonged ORR and OER reaction. These polyanionic fluorophosphates form a new class of economic and stable bifunctional electrocatalysts, with Na_2CoPO_4F delivering the best performance.

4.2. Hybrid Na–Air Battery Fabrication

The performance of hybrid metal–air batteries depends on the air cathode, where fluorophosphates with bifunctional ORR and OER activity can be a lucrative option.[246–248] Therefore, NCPF was tested as an air cathode for hybrid Na–air battery.[245] Schematic representation of hybrid Na–air battery is illustrated in Figure 13d. The high ionic conductivity of Na^+

in $Na_3Zr_2Si_2PO_{12}$ solid electrolyte combined with the high solubility of discharged product resulted in high power density and low overpotential. The complete redox reaction of the cell can be summarized as follows

$$\text{Anode}: Na^+ + e^- \leftrightarrow Na(s) \quad E^0 = -2.71\,V \tag{1}$$

$$\text{Cathode}: O_2 + 2H_2O + 4e^- \leftrightarrow 4OH^- \quad E^0 = +0.40\,V \tag{2}$$

Stable charge and discharge voltages of 2.94 and 3.34 V, respectively were recorded for 30 cycles with low overpotential. A round trip efficiency of 88% was observed showing comparable/superior performance than other reported air cathodes (Figure 13e,f). These preliminary results establish fluorophosphates as a new class of air-cathodes for rechargeable metal–air batteries.

5. Perspectives

The world is expected to see a massive growth in energy consumption in line with developments taking place in countries like India and China. In fact, the International Energy Agency estimates that India alone is likely to contribute 25% to the rise in global energy demand by 2040. To keep pace with this demand while committing to a net zero carbon emission energy system by 2050, the current energy mix that consists of over 92% fossil fuel sources needs to be aggressively transitioned toward renewable energy sources. It is widely recognized that large scale integration of renewables in the energy system mandates adequate energy storage solutions to overcome intermittency issues and to create a more robust and flexible electricity distribution system. Deploying adequate grid level energy storage is a key to break the constraint that the temporal variation in energy production rate needs to be matched by the energy consumption rate. The energy reservoir can absorb extra energy produced when demand is low and provide that energy when production is low. Such flexibility can also help with energy arbitrage, i.e., to purchase energy when demand/cost is low. Energy storage also has the potential to transform the energy distribution landscape by enabling microgrids, where individual homes, apartment buildings, universities and townships having their own energy ecosystem with a customized mix of generation, storage and immunity to power disruption. Microgrids help since the source of the problem can be easily isolated from the network. Energy storage technology is also an enabler for electric mobility that could eliminate dependency on imported oil.

In many ways, the fossil fuel based to renewables energy transition is critically dependent on access to inexpensive and reliable energy storage technology. So, what would it take to achieve the goal of making widespread deployment of energy storage technology a reality? Until now lithium-ion batteries (LIBs) have dominated energy storage technology, primarily driven by the portable electronics market. However, as demand for energy storage for electric vehicles (EV) and grid level storage applications grow, it is expected to put a severe pressure on the supply chain of raw materials used for LIBs. First of all, even though there may be enough lithium reserves in the world to cater to the global energy storage needs, lithium is highly unevenly distributed with over 75% of lithium situated in few countries like Bolivia, Chile, China, Argentina, and Australia. More critically, a majority (≈60%) of the cobalt (Co) used in LIB cathode comes from Democratic Republic of Congo. Future expansion of LIB market is expected to be hampered by the limited supply of Li and Co. Thus, there is a great risk to the expansion of the energy storage market solely based on LIB technology since availability of both Li and Co may be constrained by geopolitical issues. To avoid these issues world needs to look beyond the state-of-the-art lithium-ion battery technology. In fact, as different storage applications pose different requirements, it is imperative that varieties of battery technologies are available. In all these applications, however, the common requirements are that the storage technology be inexpensive, safe and have long operational time. For example, for grid scale applications, a price point of \$100 kWh^{-1} and a service life of 10 000 cycles/10 years is a target that makes integration of energy storage very attractive. For EV application, specific energy target of 300 Wh kg^{-1} (at the cell level) is an additional important consideration.

The promising alternatives begin with replacing Co based cathodes in current LIBs with Co free cathode materials. Further along, sodium intercalation-based chemistries, even though not as energy dense as LIBs, are very promising for grid level storage applications since they can be very cost competitive, as both sodium and the sodium intercalation materials for use in cathodes are earth abundant. Polyanionic cathode materials for LIBs and SIBs considered in this review represent these two approaches, respectively. Before we provide a more detailed account of the chemistries involved, it is worthwhile to compare different cathode materials with respect to their energy densities. The voltage versus specific capacity and specific versus volumetric energy density plots of polyanionic cathode materials for LIBs and SIBs with conventional cathode materials are compared (**Figure 14**a,b). It can be noted that the relatively high standard redox potential of Na/Na^+ leads to a lower working voltage for sodium-based materials as compared to lithium-based materials.

The energy storage technology of choice from economic and environmental point of view is highly application-dependent.[249] Energy storage technologies are evaluated on different performance parameters and no single technology excels on all. The key performance parameters, which are important in the analysis of alternative battery chemistries are: energy density, power density, round trip efficiency (RTE), cycle life and cost.[250] While the stringent requirements on power and energy densities encountered in electric vehicles and consumer electronics applications are significantly relaxed in stationary storage applications, they still determine the storage system's real estate footprint. Thus, it is desirable to have reasonably high volumetric energy densities without increasing the cost of storage. The round-trip efficiency takes into account energy losses from power conversion and is important determinant of operating cost of an energy storage system.[251] On the other hand, cost and cycle life determine the capital expenditure involved in setting up the storage system. For typical stationary storage applications, assuming one or two cycles per day, 3650–7300

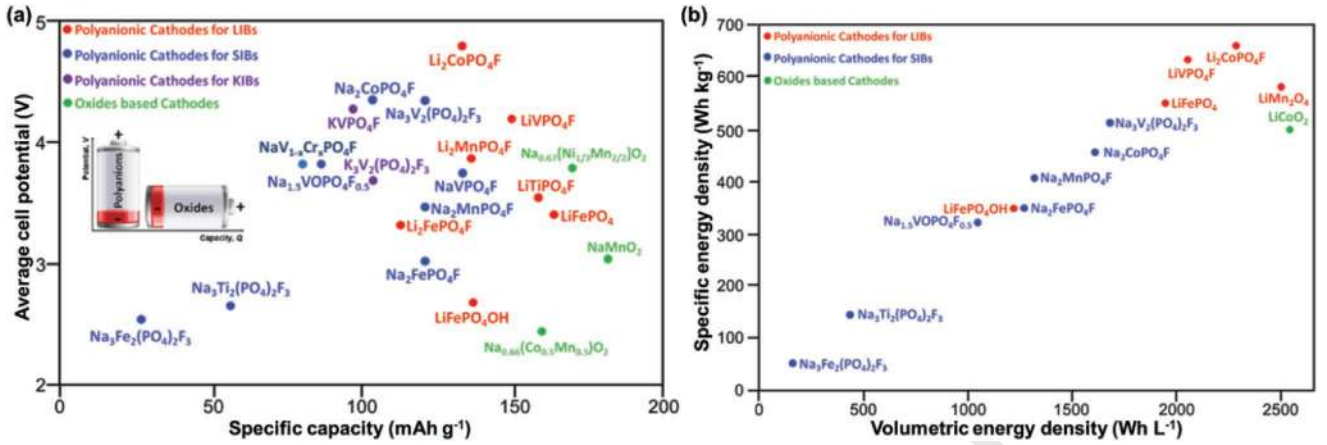

Figure 14. a) Potential versus specific capacity plot for different fluorophosphate cathode materials. b) Comparison of specific energy versus volumetric energy density of fluorophosphate cathodes with selected commercialized LIB cathodes (e.g., $LiCoO_2$).

to lifetime cycles would be adequate to allow for a 10-year operation. Before we analyze different fluorophosphate-based cathodes, it is worthwhile to note how existing battery energy storage technologies fare, as a reference. For example, Tesla's powerwall is a Li-ion based system with an RTE of 92%, a cost of \$350 kWh^{-1} and a cycle life of 10 000. In contrast, the EOS Aurora is a zinc hybrid cathode-based system with 75% RTE, a cost of \$160 kWh^{-1} and a cycle life of 5000.[252]

The performance metrics of six key fluorophosphate battery chemistries were compared on the basis of their cyclability as tabulated in **Table 2**. Lithium-ion batteries that contained $LiVPO_4F$, $LiFePO_4F$, and sodium-ion batteries that comprised $NaVPO_4F$, Na_2FePO_4F, $Na_3V_2(PO_4)_2F_3$ were used for the analysis. It is interesting to note that all six chemistries considered have >90 % RTE, with $Na_3V_2(PO_4)_2F_3$ having the highest value. Energy storage technologies based on these cathodes would thus be more efficient than most incumbent storage technologies that have RTE in the range of 70–85%. The fact that running cost savings are directly proportional to RTE is an important consideration during selection of an appropriate storage technology. The cost metric provides an indication of how attractive the material is from the cost point of view and a higher value indicates lower cost per unit energy stored. It is important to note that Fe-based cathode materials have the lowest cost in terms of capital expenditure. Further, all these fluorophosphates are capable of reversible cycling over 3000 cycles while retaining 80% capacity.

Any analysis of the alternative battery chemistries from a commercialization perspective is not complete without a discussion about the ease of manufacturability and scale-up. Generally, vanadium based materials are synthesized by solid-state route which involves synthesis of vanadium phosphate (VPO_4) precursor that is then utilized in further steps to obtain the final products. Form manufacturability point of view, such synthesis procedure adds additional steps that amounts to additional energy and time consumption. Vanadium toxicity further makes the commercialization of V-based products difficult. On the other hand, materials like Na_2FePO_4F can be synthesized using one-step method, which can be more readily scaled to yield material in bulk quantities. One-minute synthesis of Na_2FePO_4F is also reported with good electrochemical activity.[198] Iron is present in abundance inside earth's crust which implies relatively cheaper iron-based precursors. From the safety point of view as well, use of flammable organic electrolytes can be dangerous specially during short-circuiting or over charging. With this idea, Na_2FePO_4F was tested in aqueous electrolytes as well.[210] It exhibited excellent electrochemical activity. The excellent electrochemical performance of Na_2FePO_4F in aqueous electrolytes coupled with energy-savvy and economical synthesis and elemental abundance of Na (with respect to Li) makes it a strong candidate among fluorophosphates for possible commercialization targeting stationary storage applications.

To facilitate the rapid commercialization of fluorophosphate based batteries for stationary energy storage applications, we identify a roadmap with the following key research and development themes: 1) Analysis of alternate material choices for cathode: given the vast choice of fluorophosphate based cathode

Table 2. Cyclablity of different materials chosen to study their future perspective as reported in literature.

Material	Theoretical capacity [mAh g^{-1}]	Experimental capacity [mAh g^{-1}]	C-rate	% Capacity retention [cycles]	Reference
$LiVPO_4F$	156	126	1 C	90 (1000)	[79]
$LiFePO_4F$	152	128	1 C	71 (100)	[97]
$NaVPO_4F$	142.6	100	5 C	70 (2500)	[135]
Na_2FePO_4F	124.2	66.8	4 C	84.7 (1000)	[192]
$Na_3V_2(PO_4)_2F_3$	128.2	102	10 C	90 (2000)	[154]

materials, a critical comparison of energy and power capabilities, cost, cycle stability, depth of discharge (DoD), round trip efficiency and safety is necessary to make informed choice for a given application. For example, an energy storage solution used for resiliency (support large but short duration power demand due to disruption) versus energy storage solution used in renewable systems (require longer cycle duration batteries with large capacities) have different demands. The availability of a detailed analysis of what each cathode system is capable of would help make the right choice for a specific application. Such efforts should be focused on analysis of these materials considering practical realization of large format batteries and not restricted to coin cells. 2) Identification of high performance and electrochemically stable electrolytes that work efficiently with fluorophosphate materials. In addition to organic electrolytes, this effort should also entail formulating aqueous electrolytes that improve cost effectiveness and environmental benefits. It is important to find electrolytes that form thin and stable solid electrolyte interface (SEI) to minimize cell resistance and degradation. Additionally, effort is needed to ensure that electrolytes exhibit high conductivity and Li^+ or Na^+ ion transference number, which is critical in keeping the cell impedance low. Further, the cathode material should be stable against surface degradation during cycling in the given electrolyte environment. 3) Robust multiphysics based modeling tools for cell design provide device engineering capabilities to meet performance targets (e.g., for energy, power, and cyclability). For example, active material volume fraction, electrode thickness, electrolyte loading, binder volume fraction together affects power and energy densities of a cell and the performance dependence on these cell design parameters is highly nonintuitive. Robust and efficient battery modeling tools can provide powerful platforms to quickly iterate on design choices to arrive at optimal design as opposed to a time consuming iterative experimental only design process. Some such tools are electrochemical thermal models based on pseudo-2D approach or reduced order models (ROM) coupled with optimization algorithms and design realization. Additionally, these models can also help in determining round trip efficiency, achievable DoD, power and energy densities as well as assessing degradation and cycle life. 4) Finally, manufacturability should be an important consideration while developing fluorophosphate cathode materials. It is important to develop low-cost, scalable and environmentally friendly processes to ensure fast commercialization.

6. Summary

Although LIBs dominate the portable electronics market, SIBs and KIBs can be expected to play an important role in futuristic grid-level storage. Substantial development has taken place in developing new electrode materials for SIB sans KIBs in the last two decades. With the goal of having a material that is cost effective, safe, and energy dense (both high energy and high power density), a gradual shift from oxide-based materials to polyanionic materials has been taking place since the discovery of $LiFePO_4$. While oxides deliver high capacity, the polyanions exhibit high tunable redox potential with an added advantage of high structural and thermal stability. The versatility in terms of anion substitution opens the gateway to optimize the materials for specific types of applications. Fluorine, when coupled with other anionic groups changes the chemistry substantially. Thus, the last decade has seen a booming rise in the research activity on fluorophosphates. The electronegativity of F-atom coupled with inductive effect of phosphate group increases the highest occupied molecular orbital (HOMO)–lowest unoccupied molecular orbital (LUMO) gap of central metal ion and hence increases the redox voltage. Most of the materials exhibit 3D pathways for ion diffusion. Materials like $Na_3V_2(PO_4)_2F_3$ and Na_2FePO_4F exhibit high redox potential and good cyclability. Hence, we come across many full-cell based reports with good capacity and cyclability. Several fluorophosphates have also been studied in aqueous electrolytes to design economic aqueous batteries.

Fluorophosphates can also act as bifunctional electrocatalysts to realize efficient oxygen electrolysis (ORR-OER) reactions, which can be employed in (hybrid) metal–air batteries. The electrochemical activity of fluorophosphates can be improved by various strategies like ion-doping, carbon-coating, and morphology engineering. The activity can further be improved by adding suitable additives like FEC in the electrolytes in order to avoid their decomposition and SEI formation. While the vanadium-based materials can deliver high energy density, they have limited commercialization due to the toxicity of vanadium. The bottleneck for Co-based materials is the high cost of Co-based precursors. In comparison, the Ni-based materials exhibit high redox potentials, but the available electrolytes tend to decompose at higher potentials, which is an area that will require significant research in the future. The Fe-based materials are safe and cost effective due to relatively lower cost of the precursors. However, the facile oxidation of Fe^{2+} to Fe^{3+} warrants careful synthesis and material storage. Mn-based materials can offer high voltage but suffers from high polarization during cycling. Needless to say, all the materials have to be studied individually by optimizing various parameters in order to utilize the full capacity of these materials. This review is an attempt to summarize the structural and electrochemical performances of the fluorophosphates reported till date for secondary batteries. Overall, there are some challenges to be addressed in future in order to inch toward commercialization. Since most of the fluorophosphate based cathode materials exhibit high redox potential, a major challenge is to develop high voltage electrolytes capable to cycle the batteries at higher voltages enabling the activity of other available metal redox centres and increasing the energy density of the battery. The electrolyte stability can be improved either by using different solvents like dinitrile-based solvent or by adding suitable additives. Without any doubt, fluorophosphate cathodes exhibit huge potential to address the energy crisis issues at large scale level, i.e., grid storage, but more full-cell battery prototypes need to be fabricated and studied for the cycle life and stability. High temperature battery testing should also be carried out in order to see the effect of temperature on the performance. The review also pave ways for discovery and development of other fluorophosphate chemistry for (non)aqueous and metal–air batteries. Moreover, fluorophosphates can be extended to aqueous zinc battery applications. Aqueous zinc-ion batteries have witnessed a huge

uprise in terms of research recently and is considered to be important candidates for grid scale energy storage due to safety and low cost. Using water-in-bisalt aqueous electrolytes, fluorophosphate materials can be tested for aqueous (Li/Na/Zn) battery applications. On a broader note, alkali metal fluorophosphate forms a niche class of polyanionic electrode materials exhibiting rich material chemistry, structural diversity, chemical/thermal stability coupled with robust electrochemical and electrocatalytic activities, suitable for insertion-type and metal–air batteries. Some selected fluorophosphates can be close to commercialization in near future particularly targeting the stationary grid storage applications.

Acknowledgements

The first author is grateful to the Ministry of Human Resource Development (Govt. of India) for a doctorate fellowship. He also thanks the Electrochemical Society (ECS, USA) for a 2020 ECS Summer Fellowship. P.B. acknowledges the financial support from the Technology Mission Division (Department of Science and Technology, Govt. of India) under the Materials for Energy Storage (MES-2018) program (DST/TMD/MES/2k18/207). Research reported in this publication was partially supported by King Abdullah University of Science and Technology (KAUST). The material structures were illustrated using VESTA software.[253]

Conflict of interest

The authors declare no conflict of interest.

Keywords

batteries, capacity, cathodes, electrocatalysis, fluorophosphates, polyanions

Received: April 28, 2020
Revised: June 11, 2020
Published online:

[1] V. Etacheri, R. Marom, R. Elazari, G. Salitra, D. Aurbach, *Energy Environ. Sci.* **2011**, *4*, 3243.
[2] Y. Wang, B. Liu, Q. Li, S. Cartmell, S. Ferrara, Z. D. Deng, J. Xiao, *J. Power Sources* **2015**, *286*, 330.
[3] D. Larcher, J.-M. Tarascon, *Nat. Chem.* **2015**, *7*, 19.
[4] B. Scrosati, *Electrochim. Acta* **2000**, *45*, 2461.
[5] N. Nitta, F. Wu, J. T. Lee, G. Yushin, *Mater. Today* **2015**, *18*, 252.
[6] M. D. Slater, D. Kim, E. Lee, C. S. Johnson, *Adv. Funct. Mater.* **2013**, *23*, 947.
[7] N. Yabuuchi, K. Kubota, M. Dahbi, S. Komaba, *Chem. Rev.* **2014**, *114*, 11636.
[8] J.-Y. Hwang, S.-T. Myung, Y.-K. Sun, *Chem. Soc. Rev.* **2017**, *46*, 3529.
[9] C. Vaalma, D. Buchholz, M. Weil, S. Passerini, *Nat. Rev. Mater.* **2018**, *3*, 18013.
[10] K. Kubota, S. Komaba, *J. Electrochem. Soc.* **2015**, *162*, A2538.
[11] P. Barpanda, *Chem. Mater.* **2016**, *28*, 1006.
[12] A. Manthiram, J. B. Goodenough, *J. Power Sources* **1989**, *26*, 403.
[13] A. K. Padhi, V. Manivannan, J. B. Goodenough, *J. Electrochem. Soc.* **1998**, *145*, 1518.
[14] P. Barpanda, L. Lander, S. Nishimura, A. Yamada, *Adv. Energy Mater.* **2018**, *8*, 1703055.
[15] C. Masquelier, L. Croguennec, *Chem. Rev.* **2013**, *113*, 6552.
[16] B. Senthilkumar, C. Murugesan, L. Sharma, S. Lochab, P. Barpanda, *Small Methods* **2019**, *3*, 1800253.
[17] J. Barker, M. Y. Saidi, J. L. Swoyer, *J. Electrochem. Soc.* **2003**, *150*, A1394.
[18] B. L. Ellis, W. R. M. Makahnouk, Y. Makimura, K. Toghill, L. F. Nazar, *Nat. Mater.* **2007**, *6*, 749.
[19] N. Recham, J.-N. Chotard, L. Dupont, K. Djellab, M. Armand, J.-M. Tarascon, *J. Electrochem. Soc.* **2009**, *156*, A993.
[20] Y. Lu, S. Zhang, Y. Li, L. Xue, G. Xu, X. Zhang, *J. Power Sources* **2014**, *247*, 770.
[21] J. Barker, R. K. B. Gover, P. Burns, A. Bryan, M. Y. Saidi, J. L. Swoyer, *J. Power Sources* **2005**, *146*, 516.
[22] R. K. B. Gover, A. Bryan, P. Burns, J. Barker, *Solid State Ionics* **2006**, *177*, 1495.
[23] H. Kim, J. Hong, K.-Y. Park, H. Kim, S.-W. Kim, K. Kang, *Chem. Rev.* **2014**, *114*, 11788.
[24] W. Li, J. R. Dahn, D. S. Wainwright, *Science* **1994**, *264*, 1115.
[25] J. Köhler, H. Makihara, H. Uegaito, H. Inoue, M. Toki, *Electrochim. Acta* **2000**, *46*, 59.
[26] G. X. Wang, S. Zhong, D. H. Bradhurst, S. X. Dou, H. K. Liu, *J. Power Sources* **1998**, *74*, 198.
[27] W. Li, J. R. Dahn, *J. Electrochem. Soc.* **1995**, *142*, 1742.
[28] X.-H. Liu, T. Saito, T. Doi, S. Okada, J. Yamaki, *J. Power Sources* **2009**, *189*, 706.
[29] K. Mizushima, P. C. Jones, P. J. Wiseman, J. B. Goodenough, *Mater. Res. Bull.* **1980**, *15*, 783.
[30] M. Guilmard, C. Pouillerie, L. Croguennec, C. Delmas, *Solid State Ionics* **2003**, *160*, 39.
[31] T. Ohzuku, Y. Makimura, *Chem. Lett.* **2001**, *30*, 642.
[32] Z. Lu, D. D. MacNeil, J. R. Dahn, *Electrochem. Solid-State Lett.* **2001**, *4*, A191.
[33] M. M. Thackeray, C. S. Johnson, J. T. Vaughey, N. Li, S. A. Hackney, *J. Mater. Chem.* **2005**, *15*, 2257.
[34] C. Delmas, F. Cherkaoui, A. Nadiri, P. Hagenmuller, *Mater. Res. Bull.* **1987**, *22*, 631.
[35] C. Delmas, A. Nadiri, *Mater. Res. Bull.* **1988**, *23*, 65.
[36] C. Delmas, A. Nadiri, J. L. Soubeyroux, *Solid State Ionics* **1988**, *28-30*, 419.
[37] N. Ravet, J. B. Goodenough, S. Besner, M. Simoneau, P. Hovington, M. Armand, presented at Proc. of 196th Meeting of the Electrochemical Society, Honolulu, HI, **1999**, Abstract 127. Q6
[38] N. Ravet, Y. Chouinard, J. F. Magnan, S. Besner, M. Gauthier, M. Armand, *J. Power Sources* **2001**, *97–98*, 503.
[39] H. Huang, S.-C. Yin, L. F. Nazar, *Electrochem. Solid-State Lett.* **2001**, *4*, A170.
[40] A. Yamada, S.-C. Chung, K. Hinokuma, *J. Electrochem. Soc.* **2001**, *148*, A224.
[41] S. Franger, F. Le Cras, C. Bourbon, H. Rouault, *Electrochem. Solid-State Lett.* **2002**, *5*, A231.
[42] P. P. Prosini, D. Zane, M. Pasquali, *Electrochim. Acta* **2001**, *46*, 3517.
[43] F. Croce, A. d'Epifanio, J. Hassoun, A. Deptula, T. Olczac, B. Scrosati, *Electrochem. Solid-State Lett.* **2002**, *5*, A47.
[44] C. Delacourt, P. Poizot, S. Levasseur, C. Masquelier, *Electrochem. Solid-State Lett.* **2006**, *9*, A352.
[45] V. Legagneur, Y. An, A. Mosbah, R. Portal, A. L. G. La Salle, A. Verbaere, D. Guyomard, Y. Piffard, *Solid State Ionics* **2001**, *139*, 37.
[46] M. Armand, C. Michot, N. Ravet, M. Simoneau, P. Hovington, *US Patent 6085015*, **2000**.
[47] A. Nytén, A. Abouimrane, M. Armand, T. Gustafsson, J. O. Thomas, *Electrochem. Commun.* **2005**, *7*, 156.

[48] S. Nishimura, M. Nakamura, R. Natsui, A. Yamada, *J. Am. Chem. Soc.* **2010**, *132*, 13596.
[49] H. Zhou, S. Upreti, N. A. Chernova, G. Hautier, G. Ceder, M. S. Whittingham, *Chem. Mater.* **2011**, *23*, 293.
[50] H. Kim, S. Lee, Y.-U. Park, H. Kim, J. Kim, S. Jeon, K. Kang, *Chem. Mater.* **2011**, *23*, 3930.
[51] A. K. Padhi, K. S. Nanjundaswamy, C. Masquelier, S. Okada, J. B. Goodenough, *J. Electrochem. Soc.* **1997**, *144*, 1609.
[52] J. Barker, M. Y. Saidi, J. L. Swoyer, *Electrochem. Solid-State Lett.* **2003**, *6*, A1.
[53] H. Huang, T. Faulkner, J. Barker, M. Y. Saidi, *J. Power Sources* **2009**, *189*, 748.
[54] J.-M. Le Meins, M.-P. Crosnier-Lopez, A. Hemon-Ribaud, G. Courbion, *J. Solid State Chem.* **1999**, *148*, 260.
[55] J. Barker, M. Y. Saidi, J. L. Swoyer, *J. Electrochem. Soc.* **2004**, *151*, A1670.
[56] J. Barker, R. K. B. Gover, P. Burns, A. Bryan, *Electrochem. Solid-State Lett.* **2005**, *8*, A285.
[57] J. Barker, R. K. B. Gover, P. Burns, A. Bryan, M. Y. Saidi, J. L. Swoyer, *J. Electrochem. Soc.* **2005**, *152*, A1776.
[58] B. L. Ellis, T. N. Ramesh, L. J. M. Davis, G. R. Goward, L. F. Nazar, *Chem. Mater.* **2011**, *23*, 5138.
[59] J.-M. Ateba Mba, C. Masquelier, E. Suard, L. Croguennec, *Chem. Mater.* **2012**, *24*, 1223.
[60] R. J. Messinger, M. Ménétrier, E. Salager, A. Boulineau, M. Duttine, D. Carlier, J.-M. Ateba Mba, L. Croguennec, C. Masquelier, D. Massiot, *Chem. Mater.* **2015**, *27*, 5212.
[61] J. Barker, M. Y. Saidi, R. K. B. Gover, P. Burns, A. Bryan, *J. Power Sources* **2007**, *174*, 927.
[62] C. H. Chen, J. Liu, M. E. Stoll, G. Henriksen, D. R. Vissers, K. Amine, *J. Power Sources* **2004**, *128*, 278.
[63] Y. Jang, B. Huang, H. Wang, D. R. Sadoway, G. Ceder, Y. Chiang, H. Liu, H. Tamura, *J. Electrochem. Soc.* **1999**, *146*, 862.
[64] G. Ceder, Y.-M. Chiang, D. R. Sadoway, M. K. Aydinol, Y.-I. Jang, B. Huang, *Nature* **1998**, *392*, 694.
[65] Y.-I. Jang, B. Huang, H. Wang, G. R. Maskaly, G. Ceder, D. R. Sadoway, Y.-M. Chiang, H. Liu, H. Tamura, *J. Power Sources* **1999**, *81–82*, 589.
[66] L. S. Plashnitsa, E. Kobayashi, S. Okada, J. Yamaki, *Electrochim. Acta* **2011**, *56*, 1344.
[67] F. Zhou, X. Zhao, J. R. Dahn, *Electrochem. Commun.* **2009**, *11*, 589.
[68] K. Cui, S. Hu, Y. Li, *J. Power Sources* **2016**, *325*, 465.
[69] Z. Yu, L. Jiang, *Solid State Ionics* **2016**, *291*, 20.
[70] Y. Wang, H. Zhao, Y. Ji, L. Wang, Z. Wei, *Solid State Ionics* **2014**, *268*, 169.
[71] Z. Liu, W. Peng, Y. Fan, X. Li, Z. Wang, H. Guo, J. Wang, *J. Alloys Compd.* **2015**, *639*, 496.
[72] J. Wang, X. Li, Z. Wang, B. Huang, Z. Wang, H. Guo, *J. Power Sources* **2014**, *251*, 325.
[73] J. Wang, Z. Liu, G. Yan, H. Li, W. Peng, X. Li, L. Song, K. Shih, *J. Power Sources* **2016**, *329*, 553.
[74] Z. Liu, W. Peng, Z. Xu, K. Shih, J. Wang, Z. Wang, X. Lv, J. Chen, X. Li, *ChemSusChem* **2016**, *9*, 2122.
[75] X. Lv, Z. Xu, J. Li, J. Chen, Q. Liu, *J. Alloys Compd.* **2016**, *681*, 253.
[76] H. Yan, X. Wu, Y. Li, *Electrochim. Acta* **2015**, *182*, 437.
[77] E. V. Antipov, N. R. Khasanova, S. S. Fedotov, *IUCrJ* **2015**, *2*, 85.
[78] Y. Liu, Y. Xu, X. Sun, *Funct. Mater. Lett.* **2013**, *06*, 1350053.
[79] X. Sun, Y. Xu, M. Jia, P. Ding, Y. Liu, K. Chen, *J. Mater. Chem. A* **2013**, *1*, 2501.
[80] J. Wang, X. Li, Z. Wang, H. Guo, Y. Li, Z. He, B. Huang, *J. Alloys Compd.* **2013**, *581*, 836.
[81] Z. Peng, Z. Gan, K. Du, Y. Cao, X. Xie, Y. Wang, Y. Li, G. Hu, *J. Alloys Compd.* **2018**, *730*, 261.
[82] X. Sun, Y. Xu, G. Chen, P. Ding, X. Zheng, *Solid State Ionics* **2014**, *268*, 236.
[83] X. Lv, Z. Xu, J. Li, J. Chen, Q. Liu, *J. Solid State Chem.* **2016**, *239*, 228.
[84] Y. Shi, J. Luo, R. Wang, J. Zhao, Q. Xie, *Solid State Ionics* **2018**, *327*, 71.
[85] X. Yang, X. Wang, K. Wang, G. Chang, *Ceram. Int.* **2018**, *44*, 3825.
[86] J. Wu, Y. Xu, X. Sun, C. Wang, B. Zhang, J. Zhao, *J. Power Sources* **2018**, *396*, 155.
[87] J.-M. A. Mba, L. Croguennec, N. I. Basir, J. Barker, C. Masquelier, *J. Electrochem. Soc.* **2012**, *159*, A1171.
[88] Y. Piao, Y. Qin, Y. Ren, S. M. Heald, C. Sun, D. Zhou, B. J. Polzin, S. E. Trask, K. Amine, Y. Wei, *Phys. Chem. Chem. Phys.* **2014**, *16*, 3254.
[89] M. Bianchini, J. M. Ateba-Mba, P. Dagault, E. Bogdan, D. Carlier, E. Suard, C. Masquelier, L. Croguennec, *J. Mater. Chem. A* **2014**, *2*, 10182.
[90] S.-C. Yin, P. S. Herle, A. Higgins, N. J. Taylor, Y. Makimura, L. F. Nazar, *Chem. Mater.* **2006**, *18*, 1745.
[91] J. R. Long, L. S. McCarty, R. H. Holm, *J. Am. Chem. Soc.* **1996**, *118*, 4603.
[92] Y. Makimura, L. S. Cahill, Y. Iriyama, G. R. Goward, L. F. Nazar, *Chem. Mater.* **2008**, *20*, 4240.
[93] L. S. Cahill, Y. Iriyama, L. F. Nazar, G. R. Goward, *J. Mater. Chem.* **2010**, *20*, 4340.
[94] J. Barker, M. Y. Saidi, J. Swoyer, *US Patent 6,528,033* **2003**.
[95] N. Recham, J.-N. Chotard, J.-C. Jumas, L. Laffont, M. Armand, J.-M. Tarascon, *Chem. Mater.* **2010**, *22*, 1142.
[96] T. N. Ramesh, K. T. Lee, B. L. Ellis, L. F. Nazar, *Electrochem. Solid-State Lett.* **2010**, *13*, A43.
[97] D. Chen, G.-Q. Shao, B. Li, G.-G. Zhao, J. Li, J.-H. Liu, Z.-S. Gao, H.-F. Zhang, *Electrochim. Acta* **2014**, *147*, 663.
[98] M. Prabu, M. V. Reddy, S. Selvasekarapandian, G. V. S. Rao, B. V. R. Chowdari, *Electrochim. Acta* **2012**, *85*, 572.
[99] H. Y. Asl, A. Choudhury, *RSC Adv.* **2014**, *4*, 37691.
[100] N. Goubard-Bretesché, E. Kemnitz, N. Pinna, *Chem. - Eur. J.* **2019**, *25*, 6189.
[101] S. H. Fan, G. Q. Shao, C. Zhu, F. F. Ma, J. W. Mao, A. L. Zhang, G. Z. Xie, J. L. Yan, Y. Zhang, *Electrochim. Acta* **2018**, *280*, 248.
[102] J.-L. Yan, G.-Q. Shao, S.-H. Fan, C. Zhu, Y. Zhang, J. Wang, Q. Liu, *Molecules* **2019**, *24*, 1893.
[103] P. Rangaswamy, G. S. Suresh, M. K. Mahadevan, *ChemistrySelect* **2016**, *1*, 1472.
[104] P. Rangaswamy, G. S. Suresh, M. M. Kittappa, *J. Solid State Electrochem.* **2016**, *20*, 2619.
[105] I. M. Singh, I. B. Singh, M. Willert-Porada, *Int. J. Eng. Sci. Technol.* **2016**, *5*, 686.
[106] B. L. Ellis, T. N. Ramesh, W. N. Rowan-Weetaluktuk, D. H. Ryan, L. F. Nazar, *J. Mater. Chem.* **2012**, *22*, 4759.
[107] N. R. Khasanova, O. A. Drozhzhin, D. A. Storozhilova, C. Delmas, E. V. Antipov, *Chem. Mater.* **2012**, *24*, 4271.
[108] O. M. Karakulina, N. R. Khasanova, O. A. Drozhzhin, A. A. Tsirlin, J. Hadermann, E. V. Antipov, A. M. Abakumov, *Chem. Mater.* **2016**, *28*, 7578.
[109] S. Okada, M. Ueno, Y. Uebou, J. Yamaki, *J. Power Sources* **2005**, *146*, 565.
[110] Q. D. Truong, M. K. Devaraju, Y. Ganbe, T. Tomai, I. Honma, *Electrochim. Acta* **2014**, *127*, 245.
[111] J. Hadermann, A. M. Abakumov, S. Turner, Z. Hafideddine, N. R. Khasanova, E. V. Antipov, G. Van Tendeloo, *Chem. Mater.* **2011**, *23*, 3540.
[112] N. R. Khasanova, A. N. Gavrilov, E. V. Antipov, K. G. Bramnik, H. Hibst, *J. Power Sources* **2011**, *196*, 355.
[113] D. Wang, J. Xiao, W. Xu, Z. Nie, C. Wang, G. Graff, J.-G. Zhang, *J. Power Sources* **2011**, *196*, 2241.
[114] X. Wu, Z. Gong, S. Tan, Y. Yang, *J. Power Sources* **2012**, *220*, 122.

[115] J. Schoiber, R. J. F. Berger, J. Bernardi, M. Schubert, C. Yada, H. Miki, N. Hüsing, *Cryst. Growth Des.* **2016**, *16*, 4999.
[116] J. Schoiber, R. J. F. Berger, C. Yada, H. Miki, N. Hüsing, *J. Electrochem. Soc.* **2015**, *162*, A2679.
[117] T. Okumura, M. Shikano, Y. Yamaguchi, H. Kobayashi, *Chem. Mater.* **2015**, *27*, 2839.
[118] S. Amaresh, K. Karthikeyan, K. J. Kim, M. C. Kim, K. Y. Chung, B. W. Cho, Y. S. Lee, *J. Power Sources* **2013**, *244*, 395.
[119] C. Chang, Z. Huang, R. Tian, X. Jiang, C. Li, J. Feng, *J. Power Sources* **2017**, *364*, 351.
[120] S. S. Fedotov, A. A. Kabanov, N. A. Kabanova, V. A. Blatov, A. Zhugayevych, A. M. Abakumov, N. R. Khasanova, E. V. Antipov, *J. Phys. Chem. C* **2017**, *121*, 3194.
[121] S. W. Kim, D. H. Seo, H. Kim, K. Y. Park, K. Kang, *Phys. Chem. Chem. Phys.* **2012**, *14*, 3299.
[122] M. Dutreilh, C. Chevalier, M. El-Ghozzi, D. Avignant, J. M. Montel, *J. Solid State Chem.* **1999**, *142*, 1.
[123] M. Ue, K. Ida, S. Mori, *J. Electrochem. Soc.* **1994**, *141*, 2989.
[124] Y. Abu-Lebdeh, I. Davidson, *J. Electrochem. Soc.* **2009**, *156*, A60.
[125] Y. Abu-Lebdeh, I. Davidson, *J. Power Sources* **2009**, *189*, 576.
[126] M. Nagahama, N. Hasegawa, S. Okada, *J. Electrochem. Soc.* **2010**, *157*, A748.
[127] S. Lee, S. S. Park, *J. Solid State Chem.* **2013**, *204*, 329.
[128] H. Zhuo, X. Wang, A. Tang, Z. Liu, S. Gamboa, P. J. Sebastian, *J. Power Sources* **2006**, *160*, 698.
[129] Z. Liu, X. Wang, W. Ying, A. Tang, S. Yang, L. He, *Trans. Nonferrous Met. Soc. China* **2008**, *18*, 346.
[130] E. Boivin, J.-N. Chotard, T. Bamine, D. Carlier, P. Serras, V. Palomares, T. Rojo, A. Iadecola, L. Dupont, L. Bourgeois, *J. Mater. Chem. A* **2017**, *5*, 25044.
[131] C. Chang, Y. Li, W. He, G. Li, W. Guo, P. Zhu, M. Yao, J. Feng, *Mater. Lett.* **2017**, *209*, 82.
[132] M. Law, P. Balaya, *Energy Storage Mater.* **2018**, *10*, 102.
[133] M. Xu, C. J. Cheng, Q. Q. Sun, S. J. Bao, Y. B. Niu, H. He, Y. Li, J. Song, *RSC Adv.* **2015**, *5*, 40065.
[134] T. Jin, Y. Liu, Y. Li, K. Cao, X. Wang, L. Jiao, *Adv. Energy Mater.* **2017**, *7*, 1700087.
[135] P. Feng, W. Wang, J. Hou, K. Wang, S. Cheng, K. Jiang, *Chem. Eng. J.* **2018**, *353*, 25.
[136] M. Ling, F. Li, H. Yi, X. Li, G. Hou, Q. Zheng, H. Zhang, *J. Mater. Chem. A* **2018**, *6*, 24201.
[137] X. Ge, X. Li, Z. Wang, H. Guo, G. Yan, X. Wu, J. Wang, *Chem. Eng. J.* **2019**, *357*, 458.
[138] R. Malik, A. Abdellahi, G. Ceder, *J. Electrochem. Soc.* **2013**, *160*, A3179.
[139] O. V. Yakubovich, M. A. Simonov, O. K. Melnikov, *Kristallografiya* **1984**, *29*, 484.
[140] W. Song, X. Cao, Z. Wu, J. Chen, Y. Zhu, H. Hou, Q. Lan, X. Ji, *Langmuir* **2014**, *30*, 12438.
[141] C. Zhu, C. Wu, C.-C. Chen, P. Kopold, P. A. van Aken, J. Maier, Y. Yu, *Chem. Mater.* **2017**, *29*, 5207.
[142] T. Jiang, Y. J. Wei, W. C. Pan, Z. Li, X. Ming, G. Chen, C. Z. Wang, *J. Alloys Compd.* **2009**, *488*, L26.
[143] M. Bianchini, N. Brisset, F. Fauth, F. Weill, E. Elkaim, E. Suard, C. Masquelier, L. Croguennec, *Chem. Mater.* **2014**, *26*, 4238.
[144] T. Broux, B. Fleutot, R. David, A. Brüll, P. Veber, F. Fauth, M. Courty, L. Croguennec, C. Masquelier, *Chem. Mater.* **2018**, *30*, 358.
[145] J. Barker, R. K. B. Gover, P. Burns, A. J. Bryan, *Electrochem. Solid-State Lett.* **2006**, *9*, A190.
[146] R. A. Shakoor, D.-H. Seo, H. Kim, Y.-U. Park, J. Kim, S.-W. Kim, H. Gwon, S. Lee, K. Kang, *J. Mater. Chem.* **2012**, *22*, 20535.
[147] W. Song, X. Ji, Z. Wu, Y. Yang, Z. Zhou, F. Li, Q. Chen, C. E. Banks, *J. Power Sources* **2014**, *256*, 258.
[148] Z. Liu, Y.-Y. Hu, M. T. Dunstan, H. Huo, X. Hao, H. Zou, G. Zhong, Y. Yang, C. P. Grey, *Chem. Mater.* **2014**, *26*, 2513.
[149] M. Bianchini, F. Fauth, N. Brisset, F. Weill, E. Suard, C. Masquelier, L. Croguennec, *Chem. Mater.* **2015**, *27*, 3009.
[150] T. Broux, T. Bamine, L. Simonelli, L. Stievano, F. Fauth, M. Ménétrier, D. Carlier, C. Masquelier, L. Croguennec, *J. Phys. Chem. C* **2017**, *121*, 4103.
[151] I. L. Matts, S. Dacek, T. K. Pietrzak, R. Malik, G. Ceder, *Chem. Mater.* **2015**, *27*, 6008.
[152] G. Yan, S. Mariyappan, G. Rousse, Q. Jacquet, M. Deschamps, R. David, B. Mirvaux, J. W. Freeland, J.-M. Tarascon, *Nat. Commun.* **2019**, *10*, 1.
[153] Q. Liu, D. Wang, X. Yang, N. Chen, C. Wang, X. Bie, Y. Wei, G. Chen, F. Du, *J. Mater. Chem. A* **2015**, *3*, 21478.
[154] C. Shen, H. Long, G. Wang, W. Lu, L. Shao, K. Xie, *J. Mater. Chem. A* **2018**, *6*, 6007.
[155] L. Li, Y. Xu, X. Sun, S. He, L. Li, *Chem. Eng. J.* **2018**, *331*, 712.
[156] Q. Liu, X. Meng, Z. Wei, D. Wang, Y. Gao, Y. Wei, F. Du, G. Chen, *ACS Appl. Mater. Interfaces* **2016**, *8*, 31709.
[157] L. Li, X. Liu, L. Tang, H. Liu, Y.-G. Wang, *J. Alloys Compd.* **2019**, *790*, 203.
[158] T. Broux, F. Fauth, N. Hall, Y. Chatillon, M. Bianchini, T. Bamine, J. Leriche, E. Suard, D. Carlier, Y. Reynier, *Small Methods* **2019**, *3*, 1800215.
[159] L. H. B. Nguyen, T. Broux, P. S. Camacho, D. Denux, L. Bourgeois, S. Belin, A. Iadecola, F. Fauth, D. Carlier, J. Olchowka, *Energy Storage Mater.* **2019**, *20*, 324.
[160] L. H. B. Nguyen, P. Sanz Camacho, T. Broux, J. Olchowka, C. Masquelier, L. Croguennec, D. Carlier, *Chem. Mater.* **2019**, *31*, 9759.
[161] F. Sauvage, E. Quarez, J.-M. Tarascon, E. Baudrin, *Solid State Sci.* **2006**, *8*, 1215.
[162] W. Massa, O. V. Yakubovich, O. V. Dimitrova, *Solid State Sci.* **2002**, *4*, 495.
[163] A. A. Tsirlin, R. Nath, A. M. Abakumov, Y. Furukawa, D. C. Johnston, M. Hemmida, H.-A. K. von Nidda, A. Loidl, C. Geibel, H. Rosner, *Phys. Rev. B* **2011**, *84*, 14429.
[164] P. Serras, V. Palomares, A. Goni, I. G. de Muro, P. Kubiak, L. Lezama, T. Rojo, *J. Mater. Chem.* **2012**, *22*, 22301.
[165] Y. Qi, L. Mu, J. Zhao, Y. Hu, H. Liu, S. Dai, *Angew. Chem., Int. Ed.* **2015**, *54*, 9911.
[166] Y.-U. Park, D.-H. Seo, B. Kim, K.-P. Hong, H. Kim, S. Lee, R. A. Shakoor, K. Miyasaka, J.-M. Tarascon, K. Kang, *Sci. Rep.* **2012**, *2*, 1.
[167] D. Chao, C. Lai, P. Liang, Q. Wei, Y. Wang, C. Zhu, G. Deng, V. V. T. Doan-Nguyen, J. Lin, L. Mai, *Adv. Energy Mater.* **2018**, *8*, 1800058.
[168] Y.-U. Park, D.-H. Seo, H.-S. Kwon, B. Kim, J. Kim, H. Kim, I. Kim, H.-I. Yoo, K. Kang, *J. Am. Chem. Soc.* **2013**, *135*, 13870.
[169] N. Sharma, P. Serras, V. Palomares, H. E. A. Brand, J. Alonso, P. Kubiak, M. L. Fdez-Gubieda, T. Rojo, *Chem. Mater.* **2014**, *26*, 3391.
[170] Y. Park, D. Seo, H. Kim, J. Kim, S. Lee, B. Kim, K. Kang, *Adv. Funct. Mater.* **2014**, *24*, 4603.
[171] M. Xu, P. Xiao, S. Stauffer, J. Song, G. Henkelman, J. B. Goodenough, *Chem. Mater.* **2014**, *26*, 3089.
[172] M. Xu, L. Wang, X. Zhao, J. Song, H. Xie, Y. Lu, J. B. Goodenough, *Phys. Chem. Chem. Phys.* **2013**, *15*, 13032.
[173] P. Serras, V. Palomares, P. Kubiak, L. Lezama, T. Rojo, *Electrochem. Commun.* **2013**, *34*, 344.
[174] H. Jin, J. Dong, E. Uchaker, Q. Zhang, X. Zhou, S. Hou, J. Li, G. Cao, *J. Mater. Chem. A* **2015**, *3*, 17563.
[175] P. R. Kumar, Y. H. Jung, J. E. Wang, D. K. Kim, *J. Power Sources* **2016**, *324*, 421.
[176] Y. Yin, F. Xiong, C. Pei, Y. Xu, Q. An, S. Tan, Z. Zhuang, J. Sheng, Q. Li, L. Mai, *Nano Energy* **2017**, *41*, 452.
[177] Y. Qi, J. Zhao, C. Yang, H. Liu, Y. Hu, *Small Methods* **2019**, *3*, 1800111.

[178] J. Zhao, L. Mu, Y. Qi, Y.-S. Hu, H. Liu, S. Dai, *Chem. Commun.* **2015**, *51*, 7160.
[179] H. Jin, M. Liu, E. Uchaker, J. Dong, Q. Zhang, S. Hou, J. Li, G. Cao, *CrystEngComm* **2017**, *19*, 4287.
[180] M. Peng, B. Li, H. Yan, D. Zhang, X. Wang, D. Xia, G. Guo, *Angew. Chem., Int. Ed.* **2015**, *54*, 6452.
[181] B. Shen, Y. You, Y. Niu, Y. Li, C. Dai, L. Hu, B. Guo, J. Jiang, S. Bao, M. Xu, *ACS Appl. Mater. Interfaces* **2018**, *10*, 16581.
[182] Y. Hou, K. Chang, Z. Wang, S. Gu, Q. Liu, J. Zhang, H. Cheng, S. Zhang, Z. Chang, Z. Lu, *Sci. China Mater.* **2019**, *62*, 474.
[183] Z. Zhang, Z. Chen, Z. Mai, K. Peng, Q. Deng, A. Bayaguud, P. Zhao, Y. Fu, Y. Yu, C. Zhu, *Small* **2019**, *15*, 1900356.
[184] Y. Kawabe, N. Yabuuchi, M. Kajiyama, N. Fukuhara, T. Inamasu, R. Okuyama, I. Nakai, S. Komaba, *Electrochem. Commun.* **2011**, *13*, 1225.
[185] N. V. Kosova, V. R. Podugolnikov, E. T. Devyatkina, A. B. Slobodyuk, *Mater. Res. Bull.* **2014**, *60*, 849.
[186] M. Brisbois, N. Krins, R. P. Hermann, A. Schrijnemakers, R. Cloots, B. Vertruyen, F. Boschini, *Mater. Lett.* **2014**, *130*, 263.
[187] D. Cui, S. Chen, C. Han, C. Ai, L. Yuan, *J. Power Sources* **2016**, *301*, 87.
[188] L. Sharma, P. K. Nayak, E. De La Llave, H. Chen, S. Adams, D. Aurbach, P. Barpanda, *ACS Appl. Mater. Interfaces* **2017**, *9*, 34961.
[189] M. Law, V. Ramar, P. Balaya, *RSC Adv.* **2015**, *5*, 50155.
[190] R. Ling, S. Cai, D. Xie, W. Shen, X. Hu, Y. Li, S. Hua, Y. Jiang, X. Sun, *J. Mater. Sci.* **2018**, *53*, 2735.
[191] A. Langrock, Y. Xu, Y. Liu, S. Ehrman, A. Manivannan, C. Wang, *J. Power Sources* **2013**, *223*, 62.
[192] X. Deng, W. Shi, J. Sunarso, M. Liu, Z. Shao, *ACS Appl. Mater. Interfaces* **2017**, *9*, 16280.
[193] J. S. Ko, V. V. T. Doan-Nguyen, H.-S. Kim, X. Petrissans, R. H. DeBlock, C. S. Choi, J. W. Long, B. S. Dunn, *J. Mater. Chem. A* **2017**, *5*, 18707.
[194] R. Ling, S. Cai, S. Shen, X. Hu, D. Xie, F. Zhang, X. Sun, N. Yu, F. Wang, *J. Alloys Compd.* **2017**, *704*, 631.
[195] J. Yan, X. Liu, B. Li, *Electrochem. Commun.* **2015**, *56*, 46.
[196] D. Jin, H. Qiu, F. Du, Y. Wei, X. Meng, *Solid State Sci.* **2019**, *93*, 62.
[197] F. Wang, N. Zhang, X. Zhao, L. Wang, J. Zhang, T. Wang, F. Liu, Y. Liu, L. Fan, *Adv. Sci.* **2019**, *6*, 1900649.
[198] L. Sharma, A. Bhatia, L. Assaud, S. Franger, P. Barpanda, *Ionics* **2018**, *24*, 2187.
[199] D. L. Smiley, G. R. Goward, *Chem. Mater.* **2016**, *28*, 7645.
[200] I. V. Tereshchenko, D. A. Aksyonov, O. A. Drozhzhin, I. A. Presniakov, A. V. Sobolev, A. Zhugayevych, D. Striukov, K. J. Stevenson, E. Antipov, A. M. Abakumov, *J. Am. Chem. Soc.* **2018**, *140*, 3994.
[201] Q. Li, Z. Liu, F. Zheng, R. Liu, J. Lee, G. Xu, G. Zhong, X. Hou, R. Fu, Z. Chen, *Angew. Chem., Int. Ed.* **2018**, *57*, 11918.
[202] C. Shinagawa, Y. Morikawa, S. Nishimura, H. Ushiyama, A. Yamada, K. Yamashita, *J. Comput. Chem.* **2019**, *40*, 237.
[203] X. Wu, J. Zheng, Z. Gong, Y. Yang, *J. Mater. Chem.* **2011**, *21*, 18630.
[204] M. Avdeev, C. D. Ling, T. T. Tan, S. Li, G. Oyama, A. Yamada, P. Barpanda, *Inorg. Chem.* **2014**, *53*, 682.
[205] B. L. Ellis, W. R. M. Makahnouk, W. N. Rowan-Weetaluktuk, D. H. Ryan, L. F. Nazar, *Chem. Mater.* **2010**, *22*, 1059.
[206] K. Kubota, K. Yokoh, N. Yabuuchi, S. Komaba, *Electrochem* **2014**, *82*, 909.
[207] H. Zou, S. Li, X. Wu, M. J. McDonald, Y. Yang, *ECS Electrochem. Lett.* **2015**, *4*, A53.
[208] X. Lin, X. Hou, X. Wu, S. Wang, M. Gao, Y. Yang, *RSC Adv.* **2014**, *4*, 40985.
[209] H. Qin, Z. P. Song, H. Zhan, Y. H. Zhou, *J. Power Sources* **2014**, *249*, 367.
[210] L. Sharma, K. Nakamoto, R. Sakamoto, S. Okada, P. Barpanda, *ChemElectroChem* **2019**, *6*, 444.
[211] K. Nakamoto, R. Sakamoto, M. Ito, A. Kitajou, S. Okada, *Electrochem* **2017**, *85*, 179.
[212] S. Liu, L. Wang, J. Liu, M. Zhou, Q. Nian, Y. Feng, Z. Tao, L. Shao, *J. Mater. Chem. A* **2019**, *7*, 248.
[213] X. Lin, J. Huang, H. Tan, J. Huang, B. Zhang, *Energy Storage Mater.* **2019**, *16*, 97.
[214] H. Kim, D. Seo, M. Bianchini, R. J. Clément, H. Kim, J. C. Kim, Y. Tian, T. Shi, W. Yoon, G. Ceder, *Adv. Energy Mater.* **2018**, *8*, 1801591.
[215] H. Kim, J. C. Kim, S. Bo, T. Shi, D. Kwon, G. Ceder, *Adv. Energy Mater.* **2017**, *7*, 1700098.
[216] Y. Hironaka, K. Kubota, S. Komaba, *Chem. Commun.* **2017**, *53*, 3693.
[217] C. Vaalma, G. A. Giffin, D. Buchholz, S. Passerini, *J. Electrochem. Soc.* **2016**, *163*, A1295.
[218] H. Kim, D. Seo, J. C. Kim, S. Bo, L. Liu, T. Shi, G. Ceder, *Adv. Mater.* **2017**, *29*, 1702480.
[219] X. Wang, X. Xu, C. Niu, J. Meng, M. Huang, X. Liu, Z. Liu, L. Mai, *Nano Lett.* **2017**, *17*, 544.
[220] C. Liu, S. Luo, H. Huang, Z. Wang, A. Hao, Y. Zhai, Z. Wang, *Electrochem. Commun.* **2017**, *82*, 150.
[221] N. Recham, G. Rousse, M. T. Sougrati, J.-N. Chotard, C. Frayret, S. Mariyappan, B. C. Melot, J.-C. Jumas, J.-M. Tarascon, *Chem. Mater.* **2012**, *24*, 4363.
[222] S. S. Fedotov, N. R. Khasanova, A. S. Samarin, O. A. Drozhzhin, D. Batuk, O. M. Karakulina, J. Hadermann, A. M. Abakumov, E. V. Antipov, *Chem. Mater.* **2016**, *28*, 411.
[223] K. Chihara, A. Katogi, K. Kubota, S. Komaba, *Chem. Commun.* **2017**, *53*, 5208.
[224] J. W. D. Ng, M. Tang, T. F. Jaramillo, *Energy Environ. Sci.* **2014**, *7*, 2017.
[225] J. B. Goodenough, K.-S. Park, *J. Am. Chem. Soc.* **2013**, *135*, 1167.
[226] J.-M. Tarascon, *Nat. Chem.* **2010**, *2*, 510.
[227] J. Zhang, Z. Zhao, Z. Xia, L. Dai, *Nat. Nanotechnol.* **2015**, *10*, 444.
[228] K. Zeng, D. Zhang, *Prog. Energy Combust. Sci.* **2010**, *36*, 307.
[229] S. Styring, *Faraday Discuss.* **2012**, *155*, 357.
[230] R. B. Gordon, M. Bertram, T. E. Graedel, *Proc. Natl. Acad. Sci. USA* **2006**, *103*, 1209.
[231] B. Senthilkumar, Z. Khan, S. Park, I. Seo, H. Ko, Y. Kim, *J. Power Sources* **2016**, *311*, 29.
[232] H. Wan, R. Ma, X. Liu, J. Pan, H. Wang, S. Liang, G. Qiu, T. Sasaki, *ACS Energy Lett.* **2018**, *3*, 1254.
[233] C. Murugesan, S. Lochab, B. Senthilkumar, P. Barpanda, *ChemCatChem* **2018**, *10*, 1122.
[234] R. Gond, K. Sada, B. Senthilkumar, P. Barpanda, *ChemElectroChem* **2018**, *5*, 153.
[235] M. W. Kanan, D. G. Nocera, *Science* **2008**, *321*, 1072.
[236] R. Gond, D. K. Singh, M. Eswaramoorthy, P. Barpanda, *Angew. Chem.* **2019**, *131*, 8418.
[237] C.-Z. Yuan, Y.-F. Jiang, Z. Wang, X. Xie, Z.-K. Yang, A. Bin Yousaf, A.-W. Xu, *J. Mater. Chem. A* **2016**, *4*, 8155.
[238] Y. Gorlin, T. F. Jaramillo, *J. Am. Chem. Soc.* **2010**, *132*, 13612.
[239] D. Dwibedi, R. Gond, K. Sada, B. Senthilkumar, P. Barpanda, *MRS Adv.* **2018**, *3*, 1215.
[240] M. J. Lee, J. S. Kang, D. Ahn, D. Y. Chung, S. Park, Y. J. Son, J. M. Yoo, H. Shin, Y. S. Kang, N.-E. Sung, *Electrochim. Acta* **2017**, *245*, 219.
[241] L. Sharma, S. Baskar, P. Barpanda, *ECS Trans.* **2018**, *85*, 1221.
[242] T. Maiyalagan, K. A. Jarvis, S. Therese, P. J. Ferreira, A. Manthiram, *Nat. Commun.* **2014**, *5*, 3949.
[243] Z. Lu, H. Wang, D. Kong, K. Yan, P.-C. Hsu, G. Zheng, H. Yao, Z. Liang, X. Sun, Y. Cui, *Nat. Commun.* **2014**, *5*, 4345.
[244] H. Kim, J. Park, I. Park, K. Jin, S. E. Jerng, S. H. Kim, K. T. Nam, K. Kang, *Nat. Commun.* **2015**, *6*, 8253.
[245] L. Sharma, R. Gond, B. Senthilkumar, A. Roy, P. Barpanda, *ACS Catal.* **2020**, *10*, 43.

[246] M. Abirami, S. M. Hwang, J. Yang, S. T. Senthilkumar, J. Kim, W.-S. Go, B. Senthilkumar, H.-K. Song, Y. Kim, *ACS Appl. Mater. Interfaces* **2016**, *8*, 32778.
[247] Z. Khan, B. Senthilkumar, S. O. Park, S. Park, J. Yang, J. H. Lee, H.-K. Song, Y. Kim, S. K. Kwak, H. Ko, *J. Mater. Chem. A* **2017**, *5*, 2037.
[248] S. H. Sahgong, S. T. Senthilkumar, K. Kim, S. M. Hwang, Y. Kim, *Electrochem. Commun.* **2015**, *61*, 53.
[249] M. Arbabzadeh, R. Sioshansi, J. X. Johnson, G. A. Keoleian, *Nat. Commun.* **2019**, *10*, 3413.
[250] S. Sabihuddin, A. E. Kiprakis, M. Mueller, *Energies* **2015**, *8*, 172.
[251] D. M. Davies, M. G. Verde, O. Mnyshenko, Y. R. Chen, R. Rajeev, Y. S. Meng, G. Elliott, *Nat. Energy* **2019**, *4*, 42.
[252] B. Lin, W. Wu, *Energy* **2017**, *124*, 423.
[253] K. Momma, F. Izumi, *J. Appl. Crystallogr.* **2011**, *44*, 1272.

Lalit Sharma is currently a final year Integrated Ph.D. scholar at Faraday Materials Laboratory, Material Research Centre, Indian Institute of Science, Bangalore (India). Following his B.Sc. (Chemistry Hons.) degree from St. Stephens College, Delhi University (India) in 2014, he is pursuing his doctorate at the Indian Institute of Science. His research focuses on structural and electrochemical investigation of fluoro (hydroxy) phosphate-based polyanionic cathode materials for metal-ion and metal–air batteries.

Shashishekar P. Adiga obtained his Ph.D. in Materials Science and Engineering from North Carolina State University in 2003. He currently heads the Materials & Simulations team at Samsung Advanced Institute of Technology (SAIT), India in Bangalore. Prior to joining SAIT, he worked at Argonne National Laboratory, Kodak Research Labs, Lockheed Martin Advanced Technology Laboratories and Shell Technology Center. His research interests include computational materials science, materials for energy storage and conversion, automated materials discovery, functional, and device materials.

Husam Alshareef is a professor of Materials Science and Engineering at KAUST. After nearly 10 years in the semiconductor industry, he joined KAUST in 2009, where he initiated an active research group working on nanomaterial development for energy storage and electronics. He is a highly cited researcher in Materials Science, Fellow of the American Physical Society, Fellow of the Royal Society of Chemistry, and IEEE Distinguished Speaker in Nanotechnology.

Prabeer Barpanda is currently an associate professor in the Materials Research Centre at the Indian Institute of Science (IISc) Bangalore. Following his B. Engg. (NITR, India) and M.Phil. (Cambridge, UK), he completed Ph.D. from Rutgers University (USA, 2009). Following, he pursued postdoctoral work on Li-ion and Na-ion batteries at the Universite de Picardie Jules Verne (France, 2009–2010) and the University of Tokyo (Japan, 2010–2013). Since 2013, he is directing Faraday Materials Laboratory (IISc, India), an interdisciplinary group focusing on energy storage.

ADVANCED ENERGY MATERIALS

Please complete this form and return it via E-Mail to the Editorial Office:
advenergymat@wiley-vch.de

Reprint Order Form

Manuscript No.: _____

Customer No.: (if available) _____

Purchase Order No.: _____

Author: _____

Charges for Reprints in Euro (excl. VAT), prices are subject to change. Minimum order 50 copies.

No. of pages	50 copies	100 copies	150 copies	200 copies	300 copies	500 copies
1– 4	345,—	395,—	425,—	445,—	548,—	752,—
5– 8	490,—	573,—	608,—	636,—	784,—	1077,—
9–12	640,—	739,—	786,—	824,—	1016,—	1396,—
13–16	780,—	900,—	958,—	1004,—	1237,—	1701,—
17–20	930,—	1070,—	1138,—	1196,—	1489,—	2022,—
every additional 4 pages	147,—	169,—	175,—	188,—	231,—	315,—

Information regarding VAT: The charges for publication of *reprints/poster* are considered to be "supply of services" and therefore subject to German VAT. However, if you are an institutional customer outside Germany, the tax can be waived if you provide us with the valid VAT number of your company. Non-EU customers may have a VAT number starting with "EU" instead of their country code, if they are registered with the EU tax authorities. If you do not have a valid EU VAT number and you are a taxable person doing business in a non-EU country, please provide a certification from your local tax authorities confirming that you are a taxable person under local tax law. Please note that the certification must confirm that you are a taxable person and are conducting an economic activity in your country. **Note:** certifications confirming that you are a tax-exempt legal body (non-profit organization, public body, school, political party, etc.) in your country do not exempt you from paying German VAT.

Please send me send bill me for

☐ no. of reprints

☐ high-resolution PDF file (330 Euro excl. VAT)
E-mail address: _____

❖ Special Offer:

If you order 200 or more reprints you will get a PDF file for half price.

Please note: It is not permitted to present the PDF file on the internet or on company homepages.

Cover Posters (prices excl. VAT)
Posters of published covers are available in two sizes:

☐ DIN A2 42 x 60 cm / 17 x 24in (one copy: 39 Euro)

☐ DIN A1 60 x 84 cm / 24 x 33in (one copy: 49 Euro)

Postage for shipping (prices excl. VAT)
overseas +25 Euro
within Europe +15 Euro

VAT number: _____

Mail reprints / copies of the issue to:

_____
_____
_____
_____
_____

Send bill to:

_____
_____
_____
_____

☐ **I will pay by bank transfer**

☐ **I will pay by credit card**

VISA, Mastercard and AMERICAN EXPRESS

For your security please use this link (Credit Card Token Generator) to create a secure code Credit Card Token and include this number in the form instead of the credit card data. Click here:
https://www.wiley-vch.de/editorial_production/index.php

CREDIT CARD TOKEN NUMBER

						V									

_____
Date, Signature

Wiley-VCH Verlag GmbH & Co. KGaA – A company of John Wiley & Sons, Inc. -
Location of the Company: Weinheim - Trade Register: Mannheim, HRB 432833.
Chairman of the Supervisory Board: John Kritzmacher
General Partner: John Wiley & Sons GmbH, Location: Weinheim –
Trade Register Mannheim, HRB 432296 – Managing Director: Sabine Haag and Dr. Guido Herrmann

WILEY-VCH